Semi-quantitative understanding of source contribution to nitrous acid (HONO) based on 1-year continuous observation at the SORPES station in eastern China

Yuliang Liu[1,2], Wei Nie[1,2*], Zheng Xu[1,2], Tianyi Wang[1,2], Ruoxian Wang[1,2], Yuanyuan Li[1,2], Lei Wang[1,2], Xuguang Chi[1,2], and Aijun Ding[1,2]

[1]Joint International Research Laboratory of Atmospheric and Earth System Sciences, School of Atmospheric Sciences, Nanjing University, Nanjing, Jiangsu Province, China

[2] Collaborative Innovation Center of Climate Change, Jiangsu Province, China

Abstract

Nitrous acid (HONO), an important precursor of the hydroxyl radical (OH), has been long-standing recognized to be of significance to atmospheric chemistry, but its sources are still debate. In this study, we conducted continuous measurement of HONO from November 2017 to November 2018 at the SORPES station in Nanjing of eastern China. The yearly average mixing ratio of observed HONO was 0.69 ±0.58 ppb, showing a larger contribution to OH relative to ozone with a mean OH production rate of 1.16 ppb/h. To estimate the effect of combustion emissions of HONO, the emitted ratios of HONO and NO_x were derived from 55 fresh plumes ($NO/NO_x > 0.85$), with a mean value of 0.79%. During the nighttime, the chemistry of HONO was found to depend on RH, and heterogeneous reaction of NO_2 on aerosol surface was presumably responsible for HONO production. The average nighttime NO_2-to-HONO conversion frequency (C_{HONO}) was determined to be 0.0055 ± 0.0032 h^{-1} from 137 HONO formation cases. The missing source of HONO around noontime seemed to be photo-induced with an average $P_{unknown}$ of 1.04 ppb h^{-1}, based on a semi-quantitative HONO budget analysis. An over-determined system of equations was applied to obtain the monthly variations in nocturnal HONO sources. Except for burning-emitted HONO (approximately 23% of total measured HONO), the contribution of heterogeneous formation on ground surfaces was an approximately

constant proportion of 36% throughout the year. The soil emission revealed clear

seasonal variation, and contributed up to 40% of observed HONO in July and August.

A higher propensity for generating HONO on aerosol surface occurred in heavily

polluted period (about 40% of HONO in January). Our results highlight

ever-changing contributions of HONO sources, and encourage more long-term

observations to evaluate the contributions from varied sources.

1. Introduction

Nitrous acid (HONO) is a vital constituent of nitrogen cycle in the atmosphere, first

observed in the field by Perner and Platt (1979). The concentrations of HONO varied

from dozens of ppt in remote regions (Villena et al., 2011b;Meusel et al., 2016) to

several ppb in polluted urban regions (Yu et al., 2009;Tong et al., 2015). The

photolysis of HONO (R1) has been long standing as a momentous source of the

hydroxyl radicals (OH) especially during the early morning when other OH sources

are minor (Platt et al., 1980;Alicke, 2002, 2003). Even during the daytime, recent

studies have recognized the photolysis of HONO as a potentially stronger contributor

to daytime OH radicals than that of O_3 (Kleffmann, 2005;Elshorbany et al., 2009;Li et

al., 2018). Meanwhile, HONO has been found to affect adversely human heath (Jarvis

et al., 2005;Sleiman et al., 2010).

Although the significance of HONO has been given much weight, the sources of

ambient HONO are complicated and have been debated for decades. HONO can be

emitted from combustion, including vehicle exhaust, industrial exhaust and biomass

burning (Table 1).Tunnel experiments with tests for different engine types have

determined an emission ratio of $HONO/NO_x$ for traffic source, ranged in 0.3-0.8%

(Kirchstetter et al., 1996;Kurtenbach et al., 2001). The release from soil nitrite

through acidification reaction and partitioning is considered to be another primary

source of atmospheric HONO (Su et al., 2011). Soil nitrite could come from

biological nitrification and denitrification processes (Canfield et al., 2010;Oswald et

al., 2013), or be enriched via reactive uptake of HONO from the atmosphere

63   (VandenBoer et al., 2014a;VandenBoer et al., 2014b). In addition to direct emissions,

64   the vast majority of HONO is produced chemically. The recombination of NO and

65   OH (R3) is the main homogeneous reaction for supplying HONO (Pagsberg et al.,

66   1997;Atkinson, 2000), whose contribution may be significant under conditions of

67   sufficient reactants at daytime. During the nighttime, with low OH concentrations,

68   other larger sources, i.e. heterogeneous reactions of NO_2 on various surfaces, are

69   required to explain elevated mixing levels of HONO. Laboratory studies indicate that

70   NO_2 can be converted to HONO on humid surfaces (R4), being first order in NO_2 and

71   depending on various parameters including the gas phase NO_2 concentration, the

72   surface water content, and the surface area density (Kleffmann et al.,

73   1998;Finlayson-Pitts et al., 2003). Besides, the heterogeneous reduction of NO_2 with

74   surface organics (R5) is proposed to be another effective pathway to generate HONO

75   (Ammann et al., 1998;Ammann et al., 2005;Aubin and Abbatt, 2007), observed in

76   freshly emitted plumes with high concentrations of NO_x and BC (Xu et al., 2015).

77   Notably this reaction rate is drastically reduced after the first few seconds due to

78   consumption of the reactive surfaces (Kalberer et al., 1999;Kleffmann et al., 1999),

79   but this reaction could be strongly enhanced by light on photo-activated surface

80   (George et al., 2005;Stemmler et al., 2006;Stemmler et al., 2007). During the daytime,

81   heterogeneous HONO formation from the photolysis of adsorbed nitric acid (HNO_3)

82   and particulate nitrate (NO_3^-) at UV wavelengths has been found in experiments and

83   observations (Zhou et al., 2003;Zhou et al., 2011;Ye et al., 2016;Ye et al., 2017).

84   Heterogeneous processes are typically considered as the primary sources of HONO in

85   many regions yet are the most poorly understood. For NO_2 conversion to HONO on

86   surfaces (R4,R5), the uptake coefficients of NO_2 derived from different experiments

87   vary from 10^{-9} to 10^{-2} (Ammann et al., 1998;Kirchner et al., 2000;Underwood et al.,

88   2001;Aubin and Abbatt, 2007;Zhou et al., 2015). The key step to determine the

89   uptake of NO_2 or the reaction rate is still ill-defined, and we are also not certain if and

90   how the ambient natural surfaces can be reactivated by radiation. Furthermore, it has

91   become a main concern to compare the contributions of ground and aerosol surfaces

92   to HONO formation. It is so far, not well explained for the observed HONO,

93   especially during daytime. Large unknown sources of HONO were identified by many

94   studies (Su et al., 2008b;Sörgel et al., 2011;Michoud et al., 2014;Lee et al., 2016).

95

96   Benefitting from more and more studies, particularly the observations under different

97   environments (Lammel and Cape, 1996;Li et al., 2012), understanding of HONO

98   chemistry in the atmosphere has been greatly improved during the last decade.

99   However, most HONO observations were short-term campaigns with studies ranging

100   from several weeks to several months. For example, Reisinger (2000) found a linear

101   correlation between the HONO/NO_2 ratio and aerosol surface density in the polluted

102   winter atmosphere; and Nie et al. (2015) showed the influence of biomass burning

103   plumes on HONO chemistry, according to observed data during late April–June 2012;

104   while Wong et al. (2011) believed that NO_2 to HONO conversion on the ground was

105   the dominant source of HONO by analyzing vertical profiles from15 August to 20

106   September in 2006. Moreover, a theory that HONO from soil emission explained the

107   strength and diurnal variations of the missing source has been presented by Su et al.

108   (2011) based on data measured from 23 to 30 October 2004. In case the HONO

109   sources possibly exhibit temporal variability, especially seasonal differences, it is

110   challenging to draw a full picture on the basis of these short-term observations. More

111   than a year of continuous observation is needed, yet rather limited.

112

113   The Yangtze River Delta (YRD) is one of the most developed regions in eastern

114   China. Rapid urbanization and industrialization have induced severe air pollution over

115   the last three decades, particularly high concentrations of reactive nitrogen (Richter et

116   al., 2005;Rohde and Muller, 2015), including HONO (Wang et al., 2013;Nie et al.,

117   2015). In this study, we conducted HONO observations continuously from November

118   2017 to November 2018, at the Station for Observation Regional Processes and the

119   Earth System (SORPES), located in the western part of the YRD, a place that can be

120   influenced by air masses from different source regions of anthropogenic emissions,

121   biomass burning, dust and biogenic emissions (Ding et al., 2013;Ding et al., 2016).

122   Our one-year observation showed well-defined diurnal patterns and obvious season

123   variations of HONO concentrations at relatively high levels. We discussed the

124   potential mechanism of HONO production based upon semiquantitative analysis and

125   correlation studies, and paying special attention to changes in major sources of

126   HONO during different seasons.

127

128   **2. Methodology**

129

130   *2.1. Study site and instrumentation*

131

132   Continuous observation was conducted at the SORPES station at the Xianlin Campus

133   of Nanjing University (118°57′E, 32°07′N), located in the northeast suburb of Nanjing,

134   China, from November 2017 to November 2018 (Fig. S1). The easterly prevailing

135   wind and synoptic condition makes it a representative background site of Nanjing and

136   a regional downwind site of the city cluster in the YRD region. Detailed descriptions

137   for the station can be found in previous studies (Ding et al., 2013;Ding et al., 2016).

138

139   HONO was measured with a commercial long path absorption photometer instrument

140   (QUMA, Model LOPAP-03). The ambient air was sampled in two similar

141   temperature controlled stripping coils in series using a mixture reagent of 100 g

142   sulfanilamide and 1 L HCl (37% volume fraction) in 9 L pure water. In the first

143   stripping coil, all of the HONO and a fraction of interfering substances were absorbed

144   into solution, and the remaining interfering species (NO_2, HNO_3, HO_2NO_2, PAN, etc.)

145   were absorbed in the second stripping coil. After adding a reagent of 0.8 g

146   N-naphtylethylendiamine-dihydrochloride in 8 L pure water to, colored azo dyewas

147   formed in the solutions from 2 stripping coils, which were then separately detected via

148   long path absorption in special Teflon tubing. To minimize the measurement

149   interferences, the real HONO signal was the difference between the signals in the two

150   channels. Further details can be found in (Heland et al., 2001;Kleffmann et al., 2006).

151   To correct for the small drifts in instrument's baseline, the compressed air was

152   sampled every 12 h (flow rate: 1.0 L/min) to make zero measurement. A span check

153   was made using 0.04 mg/m³ nitrite (NO_2^-) solution each two weeks with a flow rate of

154 0.28 ml/min. The time resolution, detection limit, accuracy of the measurement was 5

155 min, 10 pptv, and 10%, respectively.

156

157 The NO and NO_2 levels were measured using a chemiluminescence instrument (TEI,

158 model 42i) coupled with a highly selective photolytic converter (Droplet

159 Measurement Technologies, model BLC), and the analyzer had a detection limit of 50

160 pptv for an integration time of 5 min, with precision of 4% and an uncertainty of 10%

161 (Xu et al., 2013). Ozone and CO were measured continuously using Thermo-Fisher

162 Scientific TEI 49i and TEI 48i, respectively. The fine particle mass concentration

163 ($PM_{2.5}$) was continuously measured with a combined technique of light scattering

164 photometry and beta radiation attenuation (Thermo Scientific SHARP Monitor Model

165 5030). Water soluble aerosol ions (NO_3^-, SO_4^{2-}, NH_4^+ etc.) and ammonia (NH_3) were

166 measured by a Monitor for Aerosols and Gases in ambient Air (designed and

167 manufactured by Applikon Analytical B.V., the Netherlands) with a $PM_{2.5}$ cyclone

168 inlet, in a time resolution of 1 hr. The size distribution of submicron particles (6-820

169 nm) is measured with a DMPS (differential mobility particle sizer) constructed at the

170 University of Helsinki in Finland. Meteorological measurements including relative

171 humidity (RH), wind speed, wind direction, and air temperature were recorded by

172 Automatic Weather Station (CAMPEEL co., AG1000). UVB total radiation was

173 measured by UVB radiometer (UVS-B-T UV Radiometer, KIPP &ZONEN).

174

175 *2.2. TUV model and OH estimate*

176

177 The Tropospheric Ultraviolet and Visible (TUV) Radiation Model

178 (http://www.acd.ucar.edu/TUV) was adopted to compute the photolysis frequencies,

179 which is most probably accurate in clean and cloudless days. The pivotal parameters

180 of this model were inputted as follows: the ozone density was measured by Total

181 Ozone Mapping Spectrometer (http://toms.gsfc.nasa.gov/teacher/ozoneoverhead.html);

182 the typical single scattering albedo (SSA) and Ångström exponent (Alpha) were 0.93

183 and 1.04 (Shen et al., 2018); The mean value of optical depth (AOD) at 550nm was

184 0.64, derived following an empirical relationship with $PM_{2.5}$ in Nanjing (Shao et al.,

185   2017). To reduce the error of model, we used observed UVB to correct simulated

186   results (J_{mod}) by Eq. (1).

187

$$J = \frac{UVB_{obs}}{UVB_{mod}} J_{mod} \tag{1}$$

189

190   The daytime OH concentration was calculated by applying the empirical model (Eq. 2)

191   proposed by Rohrer and Berresheim (2006), based on strong nearly linear correlations

192   of measured OH concentrations with simultaneously observed $J(O^1D)$. The coefficient

193   **a** reflects the average influence of reactants (e.g. NO_x, VOCs, ozone, H_2O) on OH at

194   the selected place for research; the exponent **b** represents the combined effects of all

195   photolytic processes on OH, for example, $J(O^1D)$, $J(NO_2)$, $J(HONO)$, $J(HCHO)$ and

196   so on; and the parameter **c** counts the light-independent OH sources. The values of

197   coefficients **a**, **b** and **c** in Eq. (2) are adopted from the OH studies in the Pearl River

198   Delta (PRD) and Beijing, China (Rohrer et al., 2014;Tan et al., 2017;Tan et al., 2018).

199   By summarizing the coefficients **a**, **b**, **c** in different OH observation campaigns (Table

200   S1), especially the almost equal slope of the OH-$J(O^1D)$ relation for different

201   locations and seasons in the polluted areas of China, we can make assumptions that

202   the comprehensive impact of reactants (e.g. NO_x and VOCs) on OH cannot compete

203   with that of UV light to OH, and the chemical environments of OH are similar. This

204   suggest that it can be a reasonable way to derive OH by using Eq. (2) in our study,

205   and the error of derived OH radicals has been assessed as not subverting the relative

206   conclusions in this study (Fig. S1(a) and Fig. S1(d)). The calculated OH

207   concentrations around noon ($J(O^1D) > 1 \times 10^{-5}$ s^{-1}) were in the range of 0.46-2.0×10^7

208   cm^{-3}, comparable to observations in Chinese urban or suburban atmospheres (Lu et al.,

209   2012;Lu et al., 2013).

210

$$[OH] = a \times (J(O^1D)/10^{-5}\,s^{-1})^b + c$$
$$a = 4.2 \times 10^6\,cm^{-3}, \; b=1$$
$$c = 1.0 \times 10^6\,cm^{-3} \text{ in summer} \qquad\qquad (2)$$
$$c = 0.6 \times 10^6\,cm^{-3} \text{ in spring, autumn}$$
$$c = 0.2 \times 10^6\,cm^{-3} \text{ in winter}$$

211

212

213 **3. Results**

214

215 *3.1. Observation overview*

216

217 We carried out continuous measurements for HONO at the SORPES station in the

218 northeast suburb of Nanjing from November 2017 to November 2018 with a mean

219 measured ambient HONO mixing level of 0.69 ±0.58 ppb (Fig. S2), within the range

220 of those in or in the vicinity of mega cities (Table 2). Fig.1 shows the seasonal pattern

221 of HONO and related parameters. The highest concentration of HONO was found in

222 winter (1.04 ± 0.75 ppb), followed by spring (0.68 ± 0.48 ppb), autumn (0.66 ±0.53

223 ppb) and summer (0.45 ± 0.37 ppb). Such seasonal variations in Nanjing are aligned

224 with that in Beijing (Hendrick et al., 2014), and are somewhat similar to those in Jinan

225 (Li et al., 2018), where the highest levels occurred in winter and the lowest levels

226 occurred in autumn, but these variations are different from those in Hongkong (Xu et

227 al., 2015) where the highest and lowest values of HONO appeared in autumn and

228 spring, respectively. The important point is that the seasonality of HONO coincides

229 with that of NO_x (or NO_2), which is believed to be the main precursor of HONO in

230 current studies.

231

232 The HONO to NO_x ratio or the HONO to NO_2 ratio has been used extensively in

233 previous researches to characterize the HONO levels and to indicate the extent of

234 heterogeneous conversion of NO_2 to HONO, since it is less influenced by convection

235 or transport processes than the individual concentration (Lammel and Cape,

236 1996;Stutz et al., 2002). When a large proportion of HONO comes from direct

237 emissions, the value of $HONO/NO_2$ usually becomes larger, falsely implying the

238 strong formation of HONO from NO_2. However, the freshly emitted air masses

239 generally have the lowest HONO/NO$_x$ ratio, meaning that HONO/NO$_x$ behaves better

240 than HONO/NO$_2$ in a way. As shown in Fig. 1(b), the low value of HONO/NO$_x$ in

241 winter is attributed to heavy emissions because we see high mixing ratios of NO

242 during this cold season (Fig. 1c), the reasons for two peaks of HONO/NO$_x$ in spring

243 and summer will be discussed in sections 3.3, 3.4 and 4.

244

245 All daily changes of HONO concentration in different seasons closely resemble a

246 cycle where HONO peaks in the early morning, and then decreases to the minimum in

247 the late afternoon, following the diurnal trend of NO$_x$ (Fig. 2). The daily variations of

248 HONO in Nanjing are like those seen in other urban areas (Villena et al., 2011a;Wang

249 et al., 2013;Michoud et al., 2014;Lee et al., 2016), but differ from observations on the

250 roadside (Rappenglück et al., 2013;Xu et al., 2015). At night, the mixing ratio of

251 HONO increases rapidly in the first few hours and then stabilizes (in spring and

252 summer) or gradually climbs to its peak in the morning rush hour (in winter and

253 autumn). The accumulation during nighttime hours suggests a significant production

254 of HONO exceeding the dry deposition of HONO. As the sun rises, the HONO sink

255 will be strengthened by photolysis and the vertical mixing processes, resulting that the

256 peak times of the diurnal patterns of HONO concentration varies in different seasons.

257 During the daytime, the rate of HONO abatement is rapid before noon and then

258 becomes progressively until HONO concentration falling to the minimum. Given that

259 the photolytic lifetime of HONO is about 10-20min at the midday (Stutz et al., 2000),

260 the considerable HONO concentration during daytime indicates the existence of

261 strong production of HONO.

262

263 From the daily variations of the HONO to NO$_x$ ratio, we can further understand the

264 behavior of HONO in the atmosphere. the HONO/NO$_x$ ratio is regularly enhanced

265 quickly before midnight then reaches a maximum during the latter half of the night.

266 According to Stutz et al. (2002), the highest HONO/NO$_x$ (or HONO/NO$_2$) is defined

267 by the balance between production and loss of HONO at each night, the conditions

268 affecting the highest achievable ratio at nighttime will be discussed in section 3.3.

269   What's interesting here is the peak of the HONO/NO$_x$ ratio in the midday sun in

270   spring, summer and autumn, and even in winter, the ratio doesn't decline but remains

271   stationary before and at noon. If the HONO sources during the daytime are consistent

272   with those at night, the minimum HONO/NO$_x$ ratio should occur at noon due to the

273   intense photochemical loss of HONO. Therefore, there must be additional sources of

274   HONO during daytime (e.g. R3). The increase of HONO/NO$_x$ with solar radiation

275   (e.g., UVB) is found in both diurnal and seasonal variations, indicating that these

276   daytime sources have a relationship with the intensity of solar radiation. We will

277   further discuss the potential daytime sources of HONO in section 3.4.

278

279   The elevated mixing ratio of HONO presents an efficient source of OH radicals

280   during daytime in Nanjing. We calculate the OH production rate from HONO, i.e.

281   P$_{OH}$(HONO), using Eq. (3). As discussed in Su et al. (2008b) and Li et al. (2014),

282   HONO produced by the reaction of NO with OH (R3) is actually a temporary

283   reservoir of OH radicals. The photolysis of HONO from this pathway only

284   regenerates OH radicals, cannot contribute to the concentrations of OH radicals. So it

285   is inappropriate to estimate the primary OH production from HONO based on

286   P$_{OH}$(HONO) derived from Eq. (3). For comparison, the OH production rate from

287   ozone photolysis, P$_{OH}$(O$_3$), is derived from Eq. (4). Only part of the O(^{1}D) atoms,

288   formed by the photolysis of O$_3$ at wavelengths below 320 nm (R7), can produce OH

289   radicals by reacting with water (R8) in the atmosphere, so we use the absolute water

290   concentration, which can be derived from relative humidity and temperature, to

291   calculate the branching ratio of O(^{1}D)(ϕ_{OH}) between R8 and R9. The reaction rate of

292   O(^{1}D) with O$_2$ is 4.0×10^{-11} cm^3 molecules^{-1} s^{-1} and the reaction rate of O(^{1}D) with N$_2$

293   is 3.1×10^{-11} cm^3 molecules^{-1} s^{-1} (Seinfeld and Pandis, 2016). In addition to the two

294   mechanisms mentioned above, there are other pathways to generate primary OH

295   radicals: the photolysis of aldehydes, mainly HCHO, can form HO$_2$ radicals, and then

296   converting to OH radicals by reacting with NO; the reactions of ozone with alkenes

297   produce OH radicals directly (Finlayson-Pitts and Pitts, 2000;Seinfeld and Pandis,

298   2016).

299

$$P_{OH}(HONO) = J(HONO)[HONO] \qquad (3)$$

$$P_{OH}(O_3) = 2J(O^1D)[O_3]\phi_{OH}$$
$$\phi_{OH} = k_8[H_2O]/(k_8[H_2O]+k_9[M]) \qquad (4)$$

$$O_3 + h\upsilon \rightarrow O(^1D) + O_2 \, (\lambda < 320nm) \qquad (R7)$$

$$O(^1D) + H_2O \rightarrow 2OH \qquad (R8)$$

$$O(^1D) + M \rightarrow O(^3P) + M \quad (M \text{ is } N_2 \text{ or } O_2) \qquad (R9)$$
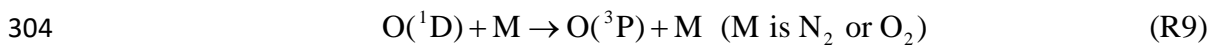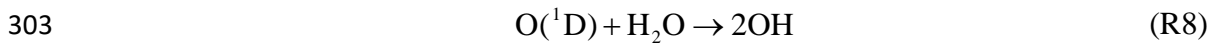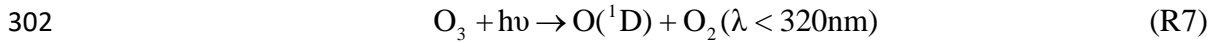
Fig. 3 shows that the diurnal peak of OH production rate from HONO is usually found in the late morning, caused by the combined effects of HONO concentration and its photolysis frequency, and the seasonal peak of $P_{OH}(HONO)$ occurs in spring for the same reason. $P_{OH}(O_3)$, coinciding with the trend of $J(O^1D)$, is highest around noon at daily time scale and is highest in summer at seasonal time scale, respectively. Significantly, the photolysis of HONO produce more OH than that of ozone throughout the daytime in winter, spring, and autumn. In summer, the contribution of HONO to OH is greater in the early morning, and although the photolysis of ozone contributes more OH at noon, the role of HONO is considerable. Overall, the average $P_{OH}(HONO)$ during 8:00-16:00 LT is 1.16 ppb/h, and the mean value of $P_{OH}(O_3)$ is 0.41 ppb/h. The impressive role of HONO in the atmospheric oxidizing capacity should benefit photochemical ozone production (Ding et al., 2013;Xu et al., 2017;Xu et al., 2018), new particle formation (Qi et al., 2015) and secondary aerosol formation (Xie et al., 2015;Sun et al., 2018) in Nanjing, the western YRD region.

3.2. Direct emissions of HONO from Combustion

As mentioned above, the good correlation of HONO with NO_x (Fig. 4a) and the similar patterns of HONO and NO_x, particularly sharply increasing together in the fresh plumes, in which the NO/NO_x ratios are usually very high (Fig. S2), indicate the presence of direct combustion emission of HONO, which need to be deducted when

327   analyzing the secondary formation of HONO. The SORPES station is influenced by

328   air masses from both industries and vehicles (Ding et al., 2016), so the traffic

329   emission factor investigated in other experiments cannot be used straightly. We derive

330   the emitted $HONO/NO_x$ ratio according the method of Xu et al. (2015), and the

331   following criteria are adopted to select fresh plumes: (a) $[NO_x] > 40$ ppbv; (b)

332     $\triangle NO / \triangle NO_x > 0.85$; (c) good correlation between HONO and NO_x (r>0.9); (d)

333   short duration of plumes (<=2 h); and (e) $[UVB] <= 0.01$ W/m^2. Then, the slopes of

334   HONO to NO_x in selected plumes were considered as the emission ratios in our study.

335

336   Within the one-year dataset, we select 55 freshly emitted plumes satisfying the criteria

337   above (Table S2), of which 20 air masses were found in the morning and evening rush

338   hours; the derived $\triangle HONO / \triangle NO_x$ ratios vary from 0.26% to 1.91% with a mean

339   value of 0.79%±0.36%. Many factors, such as the amount of excess oxygen; the types

340   of fuel used (gasoline, diesel, coal); if engines are catalyst-equipped, and if engines

341   are well-maintained, could result in variances in these ratios. Additionally, the rapid

342   heterogeneous reduction of NO_2 on synchronously emitted BC can also raise the value

343   of $\triangle HONO / \triangle NO_x$ (Xu et al., 2015). For our study, an average emission factor of

344   0.79% is deployed to evaluate the emission contribution of HONO (Eq. 5), which is

345   abbreviated as $HONO_{emis}$.

346

347 $$HONO_{emis} = NO_x \times 0.0079 \qquad (5)$$

348 $$HONO_{corr} = HONO - HONO_{emis} \qquad (6)$$

349

350   Combustion emissions contribute an average of 23% of total measured HONO

351   concentrations at night (Fig. 4b), with a maximum $HONO_{emis}/HONO$ value of 32% in

352   winter and a minimum $HONO_{emis}/HONO$ value of 18% in summer. We then get the

353   corrected observed HONO ($HONO_{corr}$) by Eq.(6) for further analysis. The slope of the

354   fitted line for HONO and NO_x is 1.62%, higher than emission ratio 0.79% (Fig. 4a),

355   and almost 80% of HONO is from $HONO_{corr}$ that is not affected by emissions (Fig.

356   4b). These imply significant secondary formation of HONO in the atmosphere.

357

3.3. Heterogeneous conversion of NO_2 to HONO during at nighttime

3.3.1. The NO_2-to-HONO conversion rate (C_{HONO})

In addition to emissions, heterogeneous reaction of NO_2 on surfaces (R4, R5) is believed to be the major formation pathways of nocturnal HONO. Thus, the NO_2-to-HONO conversion rate is calculated from Eq. (5) (Alicke et al., 2002;Alicke, 2003;Wentzell et al., 2010), where NO_2 is adopted to scale HONO to reduce the dilution influence according to Su et al. (2008a). Similar to HONO/NO_x (Fig. 2), the nighttime $HONO_{corr}$/NO_2 ratio rises from the lowest value and then reaches a quasi-stable state, meaning that C_{HONO} can actually be used to assess how quickly $HONO_{corr}$/NO_2 can increase to its equilibrium.

$$C_{HONO} = \frac{\dfrac{[HONO_{corr}]_{(t_2)}}{[NO_2]_{(t_2)}} - \dfrac{[HONO_{corr}]_{(t_1)}}{[NO_2]_{(t_1)}}}{t_2 - t_1} \tag{7}$$

Following the method of Xu et al. (2015) and Li et al. (2018), 137 cases in which $HONO_{corr}$/NO_2 increased almost linearly from 18:00 to 24:00 each night are selected, and the slope fitted by the least linear regression for $HONO_{corr}$/NO_2 against time is just the conversion frequency of NO_2 to HONO. The derived C_{HONO} vary from 0.0043 ± 0.0017 h^{-1} in winter to 0.0066 ± 0.0040 h^{-1} in summer, with an average value of 0.0055 ± 0.0032 h^{-1}, which is in the range (0.004-0.014 h^{-1}) shown by other studies in urban and suburban sites (Fig. 5). Noting that C_{HONO} assumes all the increase of $HONO_{corr}$/NO_2 is caused by the conversion of NO_2, excluding other possible sources of HONO (e.g. soil nitrite); and the computed C_{HONO} is the net NO_2-to-HONO conversion rate since the measured $HONO_{corr}$ has already taken the sinks of HONO (mainly deposition) into account. Considering the uncertainties of C_{HONO}, utilizing C_{HONO} directly to analyze the mechanism of HONO formation thoroughly may not be appropriate, but it could be attemptable to facilitate the parameterizations for HONO production in air quality models by C_{HONO} when the chemical mechanisms are not

387 clear yet.

388

389 *3.3.2. RH dependence of HONO chemistry*

390

391 It appears that NO_2 hydrolysis on humid surfaces (R4), having a first order

392 dependence on NO_2 (Jenkin et al., 1988;Ackermann, 2000;Finlayson-Pitts et al., 2003),

393 is influenced by the surface absorbed water (Kleffmann et al., 1998;Finlayson-Pitts et

394 al., 2003), although the exact mechanisms are still unknown. In the studies of Stutz et

395 al. (2002) and Stutz et al. (2004), the pseudo steady state of HONO/NO_2, where this

396 ratio is at a maximum at nighttime, is presumed to be a balance between the

397 production of HONO from NO_2 and the loss of HONO on surfaces, and the highest

398 HONO/NO_2 value is determined by the ratio of the reactive uptake coefficients for

399 each process. Scatter plot of $HONO_{corr}$/NO_2 against relative humidity in our study are

400 illustrated in Fig. 6. To eliminate as much influence of other factors as possible, the

401 average of the 6 highest $HONO_{corr}$/NO_2 values in each 5% RH interval is calculated,

402 according to Stutz et al. (2004). The phenomenon that $HONO_{corr}$/NO_2 first increases

403 and then decreases with an increasing RH in Fig. 6(a) was also observed by other

404 studies (Hao et al., 2006;Yu et al., 2009;Li et al., 2012;Wang et al., 2013). The

405 dependencies of $HONO_{corr}$/NO_2 on RH and the possible reasons or mechanisms are

406 discussed as follows. Even at the lowest measured RH of 18%, the absolute moisture

407 content in the atmosphere is still greater than 10^3 ppm in our study, which is quite

408 abundant to react with NO_2, but the $HONO_{corr}$/NO_2 ratio is quite small and remains

409 unchanged when RH is below 45%, indicating that the NO_2 to HONO conversion

410 efficiency should be determined by water covering the surfaces, rather than by the

411 amount of water in the air.

412

413 It has been reported that surfaced absorbed water depends on RH values, and the

414 dependences vary for different material surfaces of the ground, but generally follow

415 the shape of a BET isotherm (Lammel, 1999;Saliba et al., 2001;Sumner et al., 2004).

416 The number of mono-layers of water increases slowly from zero to 2-4, accompanied

417 by RH from zero to a turning point, and the water coverage grows dramatically (up to

418   10-100 mono-layers) once RH exceeds the turning point (Finlayson-Pitts et al., 2003).

419   Fig. 6(a) shows the case where the surface for NO_2 converting to HONO is dominated

420   by the ground, the $HONO_{corr}/NO_2$ increases along with RH when RH is less than 75%,

421   which can be explained by the reaction of NO_2 to generate HONO on wet surfaces.

422   However, a negative correlation between $HONO_{corr}/NO_2$ and RH is found when RH is

423   over 75%, presumably because that the rapidly growing aqueous layers of the ground

424   surface lead to efficient uptake of HONO and make the surface less accessible or less

425   reactive for NO_2. Hence, the RH turning point for absorbed water on ground surfaces

426   is perhaps around 75% for our observation, within the range of results from

427   experiments on various surfaces (70-80% RH) (Lammel, 1999;Saliba et al.,

428   2001;Sumner et al., 2004). Once RH exceeds 95%, the reaction surface is

429   asymptotically approaching the state of water droplet, where the quite limited

430   formation of HONO and the extremely impactful loss of HONO will result in a

431   dramatic decline of the $HONO_{corr}/NO_2$ ratio (Fig. 6(a) and Fig. 6(b)).

432

433   Notably, the constant $HONO_{corr}/NO_2$ value at RH between 75-95% under the

434   condition of high $PM_{2.5}$ mass loading (Fig. 6(b)), compared to the downward trend of

435    $HONO_{corr}/NO_2$ within the same humidity range in low $PM_{2.5}$ mass concentration (Fig.

436   6(a)), implies a contribution of aerosol surfaces to the NO_2-HONO conversion. Since

437   both $HONO_{corr}/NO_2$ in Fig. 6(a) and Fig. 6(b) are affected by the ground surfaces, we

438   can use the difference of $HONO_{corr}/NO_2$ between the two figures to represent the

439   influence of aerosol. As the area of shadow showed in Fig. 6(b), the aerosol-affected

440    $HONO_{corr}/NO_2$ is positively related to RH before RH reaches 95%. With the increase

441   of RH, the hygroscopic growth of aerosol particles should provide larger surface area.

442   When RH is higher than 75%, which has exceeded the mutual deliquescence relative

443   humidity of inorganic salts (Fountoukis and Nenes, 2007), aerosols will transfer to

444   aqueous phase gradually, and then promoting multiphase or heterogeneous chemistry

445   processes (Herrmann et al., 2015). For example, the oxidation of SO_2 by NO_2 on

446   aqueous aerosol surface may produce NO_2^-/HONO efficiently under polluted

447   condition (Xie et al., 2015;Wang et al., 2016). In addition, the enhancement NO_2

448   uptake on micro-droplets by anions has been reported in experiments (Yabushita et al.,

449   2009)

450

451   *3.3.3. Impact of aerosols on HONO formation*

452

453   To further understand the heterogeneous formation of HONO on aerosol, we carry out

454   a correlation analysis when $HONO_{corr}/NO_2$ reaches the pseudo steady state at each

455   night (3:00-6:00 LT). The convergence or diffusion processes of gases and particles

456   caused by the decrease or increase of the boundary layer height can also lead to a

457   consistent trend of $HONO_{corr}$ and $PM_{2.5}$ (Fig. 7a), while the ratio of $HONO_{corr}$ and

458   NO_2 can not only reduce this physical effect but also represent the conversion degree

459   of NO_2 to HONO, so a moderate positive correlation between $HONO_{corr}/NO_2$ and

460    $PM_{2.5}$ (r=0.35, p=0.01) throughout the observation period could be more convincible

461   (Fig. 7b). As shown by larger triangles with gray borders in Fig. 7(b), $HONO_{corr}/NO_2$

462   is better correlated with $PM_{2.5}$ in the months when the mass concentrations of $PM_{2.5}$

463   are higher during this 1-year measurement, generally occurring from November to

464   May (Fig. 1d).This finding can be explained with a law that greater contributions of

465   NO_2 heterogeneously reacting on aerosol surface to HONO cause better correlations

466   between $HONO_{corr}/NO_2$ and $PM_{2.5}$. Interestingly, this relationship can also be divided

467   approximately into two groups by NH_3/CO; the correlation is good when the value of

468   NH_3/CO is lower than 2‰, but when NH_3/CO is higher than 2‰, a poor correlation is

469   found. We will discuss this phenomenon further in section 4. The evidence of HONO

470   formation on aerosol were also found in other observations (Reisinger, 2000;Wang,

471   2003;Li et al., 2012;Nie et al., 2015;Hou et al., 2016;Cui et al., 2018).

472

473   As is known, producing HONO is not the dominant sink of NO_2 at night, but it seems

474   that more NO_2 can be converted to HONO under conditions of heavy pollution (Fig.

475   7b). We discuss whether heterogeneous reactions of NO_2 on aerosols are able to

476   provide comparable HONO with our measurement by Eq. (8), only considering

477   HONO formation on particle surfaces and assuming that HONO principally settles on

478 the ground surface, neglecting HONO loss on aerosol. c_{NO_2} is the mean molecular

479 velocity of NO$_2$ (370m/s); $[\frac{S}{V}]_{aer}$ is the surface area to volume ratio (m^{-1}) of aerosol;

480 ν_{HONO} is the deposition velocity of HONO, which is considered to be close to the

481 deposition velocity of NO$_2$ at night (Stutz et al., 2002;Su et al., 2008a); and a

482 approximate value of 0.1cm/s is used based on the measurements from Coe and

483 Gallagher (1992) and Stutz et al. (2002); H is the boundary layer mixing depth, and a

484 value of 100m is assumed for nighttime (Su et al., 2008a).

485

486
$$C_{HONO} = \frac{1}{4}\gamma_{NO_2 \to HONO} c_{NO_2} [\frac{S}{V}]_{aer} - \frac{\nu_{HONO}}{H} \frac{[HONO]}{[NO_2]} \quad (8)$$

487

488 Considering at nighttime period with severe haze, the aerosol surface density

489 calculated from the particle number size distributions between 6 nm and 800 nm is

490 about 1.2×10^{-3} m^{-1}, matched by 200 μg/m^3 of PM$_{2.5}$ from our observations, and the

491 averaged mixing ratios of HONO and NO$_2$ are 1.15 ppb and 28.4 ppb, respectively

492 (Table 2). For 30%-100% of the measured mean C$_{HONO}$ (0.0043 h^{-1}) in winter, the

493 uptake coefficient of NO$_2$-to-HONO ($\gamma_{NO_2 \to HONO}$) calculated from Eq. (8) is in the range

494 of 6.9×10^{-6} to 1.44×10^{-5}, consistent with the results from many laboratory studies

495 which demonstrate that the uptake coefficients of NO$_2$ (γ_{NO_2}) on multiple aerosol

496 surfaces or wet surfaces are mainly distributed around 10^{-5} with the HONO yield

497 varying from 0.1 to 0.9 (Grassian, 2002;Aubin and Abbatt, 2007;Khalizov et al.,

498 2010;Han et al., 2017). It is necessary to elaborate that: (1) the ambient particles were

499 dried with silica gel before measuring their number size distributions, and the mass

500 concentrations of PM$_{2.5}$ were also measured under a system where the temperature

501 was maintained at 30°C, usually above ambient temperature; (2) the aerosol surface

502 was calculated by assuming that all particles are spherically shaped, but the particles

503 could in fact have irregular bodies and porous structure; (3) the particle size of both

504   PM$_{2.5}$ and derived $[\dfrac{S}{V}]_{aer}$ is just a part of the total suspended particulate matter. As

505   described, the aerosol surface in the atmosphere is actually underestimated in our

506   study, thus the $\gamma_{NO_2 \to HONO}$ we derived could be the upper limit of the uptake coefficient

507   for NO$_2$ conversion to HONO on aerosol. In addition to particles surfaces, other

508   aerosol parameters such as surface water content, chemical composition, pH value,

509   and phase state of surfaces may also influence the heterogeneous formation of

510   HONO.

511

512   *3.4. Missing daytime HONO source*

513

514   After discussing the nocturnal formation mechanism of HONO, we now focus on

515   the chemistry of daytime HONO whose concentrations are still about 0.25-0.6 ppb at

516   noon with a lifetime of only 10-20 min (Fig. 2). We are not certain if the observed

517   HONO can be provided by known mechanisms (gas phase reaction (R4) and

518   emissions) to date, so a budget equation of daytime HONO (Eq. 9) is utilized to

519   analyze its source and sinks (Su et al., 2008b;Sörgel et al., 2011). Here, dHONO/dt is

520   the change rate of the observed HONO. The sources rates of HONO contain the

521   homogeneous formation rate (P$_{NO+OH}$, R3); the combustion emission rate (P$_{emis}$); and

522   the unknown HONO daytime source (P$_{unknown}$). The sink rates of HONO consist of the

523   photolysis rate (L$_{phot}$, R1); the reaction rate of HONO with OH (L$_{HONO+OH}$, R2); and

524   the dry deposition rate (L$_{dep}$). T$_V$ and T$_h$ represent the vertical (T$_V$) and horizontal (T$_h$)

525   transport processes of HONO, which are thought to be negligible for intense radiation

526   and relatively homogeneous atmospheres with generally calm winds (Dillon, 2002;Su

527   et al., 2008b;Sörgel et al., 2011).

528

529     $$\frac{dHONO}{dt} = (P_{NO+OH} + P_{emis} + P_{unknown}) - (L_{phot} + L_{HONO+OH} + L_{dep}) + T_v + T_h \qquad (9)$$

530

531   Therefore, the undiscovered daytime source of HONO (P$_{unknown}$) can be derived by Eq.

532   (10), which is a deformation of Eq. (9) without minor terms (T$_v$ and T$_h$) and where

533 dHONO/dt is substituted by ΔHONO/Δt that is counted as difference between

534 observed HONO at two time points. The reaction rate constants of reaction 2

535 ($k_{HONO+OH}$) and reaction 3 (k_{NO+OH}) are 6.0×10^{-12} cm^3 molecules^{-1} s^{-1} and 9.8×10^{-12}

536 cm^3 molecules^{-1} s^{-1}, respectively (Atkinson et al., 2004). The emission ratio of

537 HONO and NO$_x$ (HONO/NO$_x$=0.79%) obtained in section 3.2, is used to estimate

538 P_{emis}. For L_{dep}, the dry deposition velocity of diurnal HONO (v_{HONO}) is measured as

539 2cm/s in the work of Harrison et al. (1996), and a practical mixing height of 200m is

540 adopted, considering that most of the HONO cannot rise above this altitude due to

541 rapid photolysis (Alicke et al., 2002). Although we did not observe OH radicals

542 directly, the uncertainty of $P_{unknown}$ caused by the calculated OH radicals from Eq. (2)

543 can be reduced substantially in the case of low concentration of NO and high value of

544 J(O^{1}D) (Fig. S1(d)).

545

$$P_{unknown} = J(HONO)[HONO] + k_{HONO+OH}[HONO][OH] + \frac{v_{HONO}}{H}[HONO]$$
$$+ \frac{\Delta HONO}{\Delta t} - k_{NO+OH}[NO][OH] - \frac{0.79\% \times \Delta NO_x}{\Delta t} \qquad (10)$$

546

547

548 Fig. 8 shows the average daytime HONO budget from 8:00 LT to 16:00 LT during

549 different seasons. The major loss route of HONO is photodecomposition (L_{phot}) with

550 an average value of 1.50 ppb/h around noontime (10:00-14:00 LT) during this

551 observation period, next to dry deposition (L_{dep}) whose mean value at the same time is

552 0.21 ppb/h, and by $L_{HONO+OH}$ which is less than 5% of that of L_{phot}. For the sources of

553 HONO around noon, the average homogeneous reaction rate between NO and OH

554 (P_{NO+OH}) is 0.63 ppb/h and P_{emis} just gives a tiny part of HONO at a rate of 0.02 ppb/h,

555 meaning that most of HONO comes from an unknown source whose average rate

556 ($P_{unknown}$) is 1.04 ppb/h, contributing about 61% of the production of HONO.

557 Comparing summer data, the mean unknown daytime source strength of HONO in

558 Nanjing is almost at the upper-middle level of those reported in the existing literature:

559 0.22 ppb/h at a rural site of New York state, USA (Zhou et al., 2002); 0.5 ppb/h in a

560 forest near Jülich, Germany (Kleffmann, 2005); 0.77 ppb/h in a polluted rural area of

561   the Pearl River Delta, China (Li et al., 2012); 0.98 ppb/h at an urban site in Xi'an,

562   China (Huang et al., 2017); 1.7 ppb/h in an urban area of Santiago, Chile (Elshorbany

563   et al., 2009); 2.95 ppb/h in the urban atmosphere of Jinan, China (Li et al., 2018). In

564   our study, the OH production rate from the missing HONO accounts for about 53% of

565   total P_{OH}(HONO) (Fig. S2), suggesting that the unconventional source of HONO is of

566   significance to atmospheric oxidation.

567

568   Hence, we perform a correlation analysis to explore the potential unknown daytime

569   mechanisms of HONO (Table 3). $P_{unknown}$ is better correlated with NO_2*UVB than

570   with NO_2 or UVB alone in winter, spring and autumn (p=0.05), perhaps associated

571   with the photo-enhanced conversion from NO_2 to HONO (George et al.,

572   2005;Stemmler et al., 2006;Stemmler et al., 2007). The average value of $P_{unknown}$

573   normalized by NO_2 is 0.1 h^{-1}, over 18 times greater than the nighttime conversion rate

574   (0.0055 h^{-1}), also implying that $P_{unknown}$ cannot be explained by the nocturnal

575   mechanism of NO_2-to-HONO. Assuming that the height of a well-mixed boundary

576   layer around noon remains constant for each day, UVB*NO_2 and UVB*NO_2*$PM_{2.5}$

577   could be proxies for photo-induced heterogeneous reactions of NO_2 on ground and

578   aerosol surfaces, respectively. We do not have any solid evidence to identify which

579   surfaces (ground or aerosol) are more important to the photo-heterogeneous reaction

580   of NO_2 based on the present analysis. For the same reason, the photolysis of

581   particulate nitrates (NO_3^-) as a source of HONO (Ye et al., 2016;Ye et al., 2017)

582   cannot be determined whether it is momentous in our study. The comparisons of

583   correlation coefficients showed above follow the method provided by Meng et al.

584   (1992).

585

586   Our study suggest that the missing source of HONO should be considered in the air

587   quality forecasting or regional models to characterize atmospheric oxidizing capacity

588   better, especially in warm seasons (spring and summer). Based on the measurement

589   (Fig. S3), the light-induced heterogeneous conversion of NO_2 to HONO on aerosol

590   surfaces and ground surface can been included in simulation works probably, as what

591 did in Lee et al. (2016).

592

593 *4. Semi-quantitative estimation of the contribution from different sources*

594

595 From this and previous studies, we can conclude that not only the concentration of

596 ambient HONO but also the sources of HONO have temporal and spatial patterns,

597 which is supposed to be considered in model studies. Nocturnal HONO is selected to

598 discuss the monthly variations of HONO sources in detail without the uncertainties of

599 daytime HONO formation, the influences of HONO photolysis, and the mixing effect

600 of boundary layer. The heterogeneous reaction of NO_2 on aerosol produces a

601 considerable portion of HONO in relatively polluted months (Dec.-May), but

602 contributes very little less than nothing in clean months (Jun.-Oct.), as seen in section

603 3.3.3. Coincidentally, direct emissions from burning processes of HONO decrease

604 from their peak values from winter to summer (section 3.2). However, the monthly

605 averaged ratios of HONO and NO_x are highest in summer, which conflicts with the

606 two sources mentioned above.

607

608 As is known, higher NO_2-to-HONO conversion level or other NO_x-independent

609 sources can cause an increase in the HONO/NO_x ratio. For the case of a mostly

610 constant surface with low reactivity due to the prolong exposure to oxidizing gases

611 and radiation, the yield of nighttime HONO from NO_2 reacting on ground surfaces

612 could be imprecisely assumed to be unchanged. Thus, soil nitrite formed through

613 microbial activities, especially nitrification by ammonia-oxidizing bacteria

614 ($NH_4^+ \rightarrow NO_2^-$) (Su et al., 2011;Oswald et al., 2013), is adopted to be an source for

615 atmospheric HONO in this study, considering the nearby presence of some grassland

616 and natural vegetation mosaics. Although we do not directly measure HONO

617 emissions from soil, the observed ammonia can represent its monthly average

618 intensity indirectly, based on the following hypothesis: the dominant source of NH_3 is

619 from soil, especially from fertilizers ($NH_4^+ \rightarrow NH_3$) for a good correlation between

620 ammonia and temperature in the site (r=0.63, p=0.01), omitting the contributions of

621 livestock to NH_3 since there is only a small poultry facility within 10 km of this site

(Meng et al., 2011;Huang et al., 2012;Behera et al., 2013). Combustion sources (vehicles, industry, biomass burning) should contribute only a fraction of NH_3 seeing that NH_3 is not related to NOx or CO in our study. Moreover, the release of both HONO and NH_3 depend on the strength of microbial activities, fertilizing amount, and soil properties (e.g., temperature, acidity and water content of soil). Although the processes of HONO and NH_3 emission from soil may not be completely synchronized, the seasonal patterns for each should be consistent.

Until now, we can separate the sources of HONO into four parts: (1) the combustion emissions from vehicles and industries ($HONO_{emi}$) with a constant emitted HONO/NOx ratio of 0.79%; (2) the conversion of NO_2 to HONO on the ground surfaces ($HONO_{grd}$) with a constant but unknown yield x_1; (3) the conversion of NO_2 to HONO on aerosol surfaces ($HONO_{aer}$) with a $PM_{2.5}$-dependent yield ($HONO_{aer}/NO_2$); and (4) emission from soil ($HONO_{soi}$), expressed by corrected NH_3 multiplied by an unknown coefficient x_2. The corrected NH_3 is obtained by subtracting combustion emission from total observed ammonia. Ammonia from combustion is found to be proportional to simultaneous CO (Meng et al., 2011;Chang et al., 2016), and a proportion of 0.3%, which is in the lower quantile of the NH_3/CO ratios in fresh air masses (for hourly data: $NO/NO_x>0.75$; UVB=0; temperature<5°C) is used from our measurements. Substituting monthly average values of measured HONO, NO_2, $PM_{2.5}$, NH_3, and CO into Eq.(11) by assuming that $HONO_{tot}$ is equal to $HONO_{obs}$, we can get an overdetermined system of equations, which have 11 equations with 2 unknowns (excluding mean values of related parameters from February), and then we derive an approximate solution (x_1=1.89%, x_2=1.62%) by the method of ordinary least squares.

Fig. 9 shows that an average of 36% of HONO is produced heterogeneously on ground surfaces without perceptible temporal variations, but the contribution of this source is overtaken by NO_2 converting to HONO on aerosols in January (approximately 40% of HONO), and was exceeded by soil emission in July and

652 August (approximately 40% of HONO). The seasonal variations of HONO from

653 different pathways at night indicate that short-term observations may just capture a

654 small part of the total picture when exploring the source mechanisms of HONO. The

655 total HONO concentration ($HONO_{tot}$) is the sum of derived HONO from the four

656 sources listed above. The good correlation between $HONO_{tot}$ and $HONO_{obs}$ and the

657 low mean normalized error of $HONO_{tot}$ to $HONO_{obs}$ reveal that our assumption on

658 nocturnal HONO sources is reasonable. It should be noted that the slope of the

659 linearly fitted line between $HONO_{corr}/NO_2$ and $PM_{2.5}$ in spring (r=0.74, slope=0.68‰)

660 is much higher than that in winter (r=0.60, slope=0.20‰), but we just use a mean

661 slope of 0.26‰ to evaluate aerosol effects throughout the year, this may be why our

662 method underestimates HONO in March and April and overestimates HONO in

663 January, and indicating that the mass concentration of $PM_{2.5}$ is not the only factor

664 affecting formation of HONO on aerosols. Besides, lacking considerations of the

665 impact of RH and temperature on NO_2-to-HONO conversion and of seasonal

666 variations in ground surface properties, uncertainties of NO_2-to-HONO conversion

667 mechanisms and of combustion HONO emissions, and lacking direct observation for

668 soil emitted HONO, could all result in the bias between $HONO_{tot}$ and $HONO_{obs}$, so

669 more studies on the detailed mechanism of various HONO sources need to be

670 performed.

671

672
$$\frac{[HONO_{grd}]}{[NO_2]} = x_1$$
$$\frac{[HONO_{aer}]}{[NO_2]} = 0.26‰ \times [PM_{2.5}]$$
$$\frac{[HONO_{emi}]}{[NO_x]} = 0.79\%$$
$$\frac{[HONO_{soi}]}{[NH_3] - 0.3\% \times [CO]} = x_2$$
$$[HONO_{tot}] = [HONO_{emi}] + [HONO_{soi}] + [HONO_{grd}] + [HONO_{aer}]$$
(11)

673

674 *5. Conclusions*

675

676 Continuous field measurement of HONO over 1 year was conducted at the SORPES

station in Nanjing in the western YRD of China, from December 2017 to December2018. The observed seasonal average concentrations of HONO are in the range of 0.45-1.04 ppb, which are comparable to those in other urban or suburban regions and appears to be of vital importance to atmospheric oxidation as the OH production rate of HONO is almost 3 times as that of ozone at daytime. HONO and NO_x have coincident monthly variations peaking in December and decreasing to the lowest value in August, and have similar diurnal pattern with the highest value in the early morning and a low point in the late afternoon, both indicating that NO_x is a crucial precursor of HONO.

Combustion emissions contribute an average of 23% to nocturnal HONO concentrations, with an average emission ratio $\triangle HONO/\triangle NO_x$ of 0.79%. During the nighttime, the dominant source of RH-dependent HONO could be the heterogeneous reaction of NO_2 on wet ground or aerosol surfaces with a mean estimated conversion rate of 0.0055 h^{-1}. During the daytime, a missing HONO source with an average strength of 1.04 ppb/h was identified around noon, contributing about 61% of the production of HONO and seeming to be photo-enhanced. HONO released from soil is adopted to discuss the seasonal changes of nocturnal HONO, and can contribute 40% to HONO during summer. Ground formation provides a major part of HONO at a roughly constant proportion of 36%. The uptake of NO_2 on aerosol surface could generate the greatest amount of HONO during heavily polluted periods (e.g. January). Our results draw a complete picture of the sources of HONO during different seasons, and demonstrated the needs of long-term and comprehensive observations to improve the understanding of HONO chemistry.

Data availability. Measurement data at SORPES, including HONO data and relevant trace gases and aerosol data as well as meteorological data, are available upon request from the corresponding author before the SORPES database is open to the public.

706 *Author contribution.* W.N. and A.D. designed the study; Y.L. and W.N. wrote the

707 manuscript; Y.L., Z.X. and R.X. collected the HONO data and contributed to the data

708 analysis; T.W., Y.L., L.W. and X.C. collected other related data, e.g. NH_3, NO_x and

709 $PM_{2.5}$.

710

711 *Competing interests.* The authors declare that they have no conflict of interest.

712

713 *Acknowledgments.* This work was mainly funded by the National Key R&D Program

714 of China (2016YFC0202000 and 2016YFC0200500), the National Natural Science

715 Foundation of China (NSFC) project (D0512/41675145 and D0510/41605098), and

716 Jiangsu Provincial Science Fund (BK20160620). Data analysis was also supported by

717 other NSFC projects (D0512/41875175 and D0510/91644218).

References

720 Acker, K., Febo, A., Trick, S., Perrino, C., Bruno, P., Wiesen, P., Möller, D., Wieprecht, W.,
721 Auel, R., and Giusto, M.: Nitrous acid in the urban area of Rome, Atmos. Environ., 40,
722 3123-3133, 2006.
723 Ackermann, R.: Auswirkungen von Kraftfahrzeugemissionen in der urbanen Atmosphäre,
724 Dissertation. de, 2000.
725 Alicke, B.: Impact of nitrous acid photolysis on the total hydroxyl radical budget during the
726 Limitation of Oxidant Production/Pianura Padana Produzione di Ozono study in Milan,
727 Journal of Geophysical Research, 107, 10.1029/2000jd000075, 2002.
728 Alicke, B., Platt, U., and Stutz, J.: Impact of nitrous acid photolysis on the total hydroxyl
729 radical budget during the Limitation of Oxidant Production/Pianura Padana Produzione di
730 Ozono study in Milan, Journal of Geophysical Research: Atmospheres, 107, LOP 9-1-LOP
731 9-17, 2002.
732 Alicke, B.: OH formation by HONO photolysis during the BERLIOZ experiment, Journal of
733 Geophysical Research, 108, 10.1029/2001jd000579, 2003.
734 Ammann, M., Kalberer, M., Jost, D., Tobler, L., Rossler, E., Piguet, D., Gaggeler, H., and
735 Baltensperger, U.: Heterogeneous production of nitrous acid on soot in polluted airmasses,
736 NATURE, 395, 157-160, 10.1038/25965, 1998.
737 Ammann, M., Rossler, E., Strekowski, R., and George, C.: Nitrogen dioxide multiphase
738 chemistry: uptake kinetics on aqueous solutions containing phenolic compounds, Phys Chem
739 Chem Phys, 7, 2513-2518, 10.1039/b501808k, 2005.
740 Atkinson, R.: Atmospheric chemistry of VOCs and NOx, Atmos. Environ., 34, 2063-2101,
741 2000.

742 Atkinson, R., Baulch, D., Cox, R., Crowley, J., Hampson, R., Hynes, R., Jenkin, M., Rossi,
743 M., and Troe, J.: Evaluated kinetic and photochemical data for atmospheric chemistry:
744 Volume I-gas phase reactions of O x, HO x, NO x and SO x species, Atmospheric chemistry
745 and physics, 4, 1461-1738, 2004.
746 Aubin, D. G., and Abbatt, J. P.: Interaction of NO2 with hydrocarbon soot: Focus on HONO
747 yield, surface modification, and mechanism, The Journal of Physical Chemistry A, 111,
748 6263-6273, 2007.
749 Behera, S. N., Sharma, M., Aneja, V. P., and Balasubramanian, R.: Ammonia in the
750 atmosphere: a review on emission sources, atmospheric chemistry and deposition on
751 terrestrial bodies, Environ Sci Pollut Res Int, 20, 8092-8131, 10.1007/s11356-013-2051-9,
752 2013.
753 Bernard, F., Cazaunau, M., Grosselin, B., Zhou, B., Zheng, J., Liang, P., Zhang, Y., Ye, X.,
754 Daele, V., Mu, Y., Zhang, R., Chen, J., and Mellouki, A.: Measurements of nitrous acid
755 (HONO) in urban area of Shanghai, China, Environ Sci Pollut Res Int, 23, 5818-5829,
756 10.1007/s11356-015-5797-4, 2016.
757 Canfield, D. E., Glazer, A. N., and Falkowski, P. G.: The Evolution and Future of Earth's
758 Nitrogen Cycle, Science, 330, 192-196, 10.1126/science.1186120, 2010.
759 Chang, Y., Zou, Z., Deng, C., Huang, K., Collett, J. L., Lin, J., and Zhuang, G.: The
760 importance of vehicle emissions as a source of atmospheric ammonia in the megacity of
761 Shanghai, Atmospheric Chemistry and Physics, 16, 3577, 2016.
762 Coe, H., and Gallagher, M.: Measurements of dry deposition of NO2 to a Dutch heathland
763 using the eddy-correlation technique, Quarterly Journal of the Royal Meteorological Society,
764 118, 767-786, 1992.
765 Cui, L., Li, R., Zhang, Y., Meng, Y., Fu, H., and Chen, J.: An observational study of nitrous
766 acid (HONO) in Shanghai, China: The aerosol impact on HONO formation during the haze
767 episodes, Sci Total Environ, 630, 1057-1070, 10.1016/j.scitotenv.2018.02.063, 2018.
768 Dillon, M. B.: Chemical evolution of the Sacramento urban plume: Transport and oxidation,
769 2002.
770 Ding, A., Nie, W., Huang, X., Chi, X., Sun, J., Kerminen, V.-M., Xu, Z., Guo, W., Petäjä, T.,
771 Yang, X., Kulmala, M., and Fu, C.: Long-term observation of air pollution-weather/climate
772 interactions at the SORPES station: a review and outlook, Frontiers of Environmental Science
773 & Engineering, 10, 10.1007/s11783-016-0877-3, 2016.
774 Ding, A. J., Fu, C. B., Yang, X. Q., Sun, J. N., Zheng, L. F., Xie, Y. N., Herrmann, E., Nie,
775 W., Petäjä, T., Kerminen, V. M., and Kulmala, M.: Ozone and fine particle in the western
776 Yangtze River Delta: an overview of 1 yr data at the SORPES station, Atmospheric
777 Chemistry and Physics, 13, 5813-5830, 10.5194/acp-13-5813-2013, 2013.
778 Dusanter, S., Vimal, D., Stevens, P., Volkamer, R., and Molina, L.: Measurements of OH and
779 HO2 concentrations during the MCMA-2006 field campaign–Part 1: Deployment of the
780 Indiana University laser-induced fluorescence instrument, Atmospheric Chemistry and
781 Physics, 9, 1665-1685, 2009.
782 Elshorbany, Y. F., Kurtenbach, R., Wiesen, P., Lissi, E., Rubio, M., Villena, G., Gramsch, E.,
783 Rickard, A., Pilling, M., and Kleffmann, J.: Oxidation capacity of the city air of Santiago,
784 Chile, Atmospheric Chemistry and Physics, 9, 2257-2273, 2009.
785 Finlayson-Pitts, B. J., and Pitts, J. N.: CHAPTER 6 - Rates and Mechanisms of Gas-Phase

Reactions in Irradiated Organic – NOx – Air Mixtures, in: Chemistry of the Upper and Lower Atmosphere, edited by: Finlayson-Pitts, B. J., and Pitts, J. N., Academic Press, San Diego, 179-263, 2000.

Finlayson-Pitts, B. J., Wingen, L. M., Sumner, A. L., Syomin, D., and Ramazan, K. A.: The heterogeneous hydrolysis of NO2 in laboratory systems and in outdoor and indoor atmospheres: An integrated mechanism, Physical Chemistry Chemical Physics, 5, 223-242, 10.1039/b208564j, 2003.

Fountoukis, C., and Nenes, A.: ISORROPIA II: a computationally efficient thermodynamic equilibrium model for K+-Ca2+-Mg2+-Nh(4)(+)-Na+-SO42--NO3--Cl--H2O aerosols, Atmospheric Chemistry and Physics, 7, 4639-4659, 10.5194/acp-7-4639-2007, 2007.

George, C., Strekowski, R. S., Kleffmann, J., Stemmler, K., and Ammann, M.: Photoenhanced uptake of gaseous NO2 on solid organic compounds: a photochemical source of HONO?, Faraday Discussions, 130, 195, 10.1039/b417888m, 2005.

Grassian, V.: Chemical reactions of nitrogen oxides on the surface of oxide, carbonate, soot, and mineral dust particles: Implications for the chemical balance of the troposphere, The Journal of Physical Chemistry A, 106, 860-877, 2002.

Han, C., Liu, Y., and He, H.: Heterogeneous reaction of NO2 with soot at different relative humidity, Environmental Science and Pollution Research, 24, 21248-21255, 10.1007/s11356-017-9766-y, 2017.

Hao, N., Zhou, B., Chen, D., and Chen, L.-m.: Observations of nitrous acid and its relative humidity dependence in Shanghai, Journal of Environmental Sciences, 18, 910-915, 10.1016/s1001-0742(06)60013-2, 2006.

Harrison, R. M., Peak, J. D., and Collins, G. M.: Tropospheric cycle of nitrous acid, Journal of Geophysical Research: Atmospheres, 101, 14429-14439, 1996.

Heland, J., ., Kleefmann, J., ., Kurtenbach, R., ., and Wiesen, P., . A new instrument to measure gaseous nitrous acid (HONO) in the atmosphere, Environmental Science & Technology, 35, 3207-3212, 2001.

Hendrick, F., Müller, J. F., Clémer, K., Wang, P., De Mazière, M., Fayt, C., Gielen, C., Hermans, C., Ma, J. Z., Pinardi, G., Stavrakou, T., Vlemmix, T., and Van Roozendael, M.: Four years of ground-based MAX-DOAS observations of HONO and NO₂ in the Beijing area, Atmospheric Chemistry and Physics, 14, 765-781, 10.5194/acp-14-765-2014, 2014.

Herrmann, H., Schaefer, T., Tilgner, A., Styler, S. A., Weller, C., Teich, M., and Otto, T.: Tropospheric aqueous-phase chemistry: kinetics, mechanisms, and its coupling to a changing gas phase, Chem Rev, 115, 4259-4334, 10.1021/cr500447k, 2015.

Hou, S., Tong, S., Ge, M., and An, J.: Comparison of atmospheric nitrous acid during severe haze and clean periods in Beijing, China, Atmos. Environ., 124, 199-206, 10.1016/j.atmosenv.2015.06.023, 2016.

Huang, R. J., Yang, L., Cao, J., Wang, Q., Tie, X., Ho, K. F., Shen, Z., Zhang, R., Li, G., Zhu, C., Zhang, N., Dai, W., Zhou, J., Liu, S., Chen, Y., Chen, J., and O'Dowd, C. D.: Concentration and sources of atmospheric nitrous acid (HONO) at an urban site in Western China, Sci Total Environ, 593-594, 165-172, 10.1016/j.scitotenv.2017.02.166, 2017.

Huang, X., Song, Y., Li, M., Li, J., Huo, Q., Cai, X., Zhu, T., Hu, M., and Zhang, H.: A high-resolution ammonia emission inventory in China, Global Biogeochemical Cycles, 26,

830 n/a-n/a, 10.1029/2011gb004161, 2012.

831 Jarvis, D. L., Leaderer, B. P., Chinn, S., and Burney, P. G.: Indoor nitrous acid and
832 respiratory symptoms and lung function in adults, Thorax, 60, 474-479,
833 10.1136/thx.2004.032177, 2005.

834 Jenkin, M. E., Cox, R. A., and Williams, D. J.: Laboratory studies of the kinetics of formation
835 of nitrous acid from the thermal reaction of nitrogen dioxide and water vapour, Atmos.
836 Environ., 22, 487-498, 1988.

837 Kalberer, M., Ammann, M., Arens, F., Gäggeler, H. W., and Baltensperger, U.:
838 Heterogeneous formation of nitrous acid (HONO) on soot aerosol particles, Journal of
839 Geophysical Research: Atmospheres, 104, 13825-13832, 10.1029/1999jd900141, 1999.

840 Kanaya, Y., Cao, R., Akimoto, H., Fukuda, M., Komazaki, Y., Yokouchi, Y., Koike, M.,
841 Tanimoto, H., Takegawa, N., and Kondo, Y.: Urban photochemistry in central Tokyo: 1.
842 Observed and modeled OH and HO2radical concentrations during the winter and summer of
843 2004, Journal of Geophysical Research, 112, 10.1029/2007jd008670, 2007.

844 Khalizov, A. F., Cruz-Quinones, M., and Zhang, R.: Heterogeneous reaction of NO2 on fresh
845 and coated soot surfaces, The Journal of Physical Chemistry A, 114, 7516-7524, 2010.

846 Kirchner, U., Scheer, V., and Vogt, R.: FTIR spectroscopic investigation of the mechanism
847 and kinetics of the heterogeneous reactions of NO2 and HNO3 with soot, The Journal of
848 Physical Chemistry A, 104, 8908-8915, 2000.

849 Kirchstetter, T., Harley, R., and Littlejohn, D.: Measurement of Nitrous Acid in Motor
850 Vehicle Exhaust, Environmental Science & Technology Letters, 30, 2843-2849,
851 10.1021/es960135y, 1996.

852 Kleffmann, J., Becker, K., and Wiesen, P.: Heterogeneous NO2 conversion processes on acid
853 surfaces: Possible atmospheric implications, Atmos. Environ., 32, 2721-2729,
854 10.1016/S1352-2310(98)00065-X, 1998.

855 Kleffmann, J., Becker, K. H., Lackhoff, M., and Wiesen, P.: Heterogeneous conversion of
856 NO2 on carbonaceous surfaces, Physical Chemistry Chemical Physics, 1, 5443-5450, 1999.

857 Kleffmann, J.: Daytime formation of nitrous acid: A major source of OH radicals in a forest,
858 Geophysical Research Letters, 32, 10.1029/2005gl022524, 2005.

859 Kleffmann, J., Lörzer, J. C., Wiesen, P., Kern, C., Trick, S., Volkamer, R., Rodenas, M., and
860 Wirtz, K.: Intercomparison of the DOAS and LOPAP techniques for the detection of nitrous
861 acid (HONO), Atmos. Environ., 40, 3640-3652, 10.1016/j.atmosenv.2006.03.027, 2006.

862 Kurtenbach, R., Becker, K., Gomes, J., Kleffmann, J., Lorzer, J., Spittler, M., Wiesen, P.,
863 Ackermann, R., Geyer, A., and Platt, U.: Investigations of emissions and heterogeneous
864 formation of HONO in a road traffic tunnel, Atmos. Environ., 35, 3385-3394,
865 10.1016/S1352-2310(01)00138-8, 2001.

866 Lammel, G., and Cape, J. N.: Nitrous Acid and Nitrite in the Atmosphere, CHEMICAL
867 SOCIETY REVIEWS, 25, 361-369, 10.1039/cs9962500361, 1996.

868 Lammel, G.: Formation of nitrous acid: parameterisation and comparison with observations,
869 Max-Planck-Institut für Meteorologie, 1999.

870 Lee, J. D., Whalley, L. K., Heard, D. E., Stone, D., Dunmore, R. E., Hamilton, J. F., Young,
871 D. E., Allan, J. D., Laufs, S., and Kleffmann, J.: Detailed budget analysis of HONO in central
872 London reveals a missing daytime source, Atmospheric Chemistry and Physics, 16,
873 2747-2764, 10.5194/acp-16-2747-2016, 2016.

874 Li, D., Xue, L., Wen, L., Wang, X., Chen, T., Mellouki, A., Chen, J., and Wang, W.:
875 Characteristics and sources of nitrous acid in an urban atmosphere of northern China: Results
876 from 1-yr continuous observations, Atmos. Environ., 182, 296-306,
877 10.1016/j.atmosenv.2018.03.033, 2018.
878 Li, X., Brauers, T., Häseler, R., Bohn, B., Fuchs, H., Hofzumahaus, A., Holland, F., Lou, S.,
879 Lu, K. D., Rohrer, F., Hu, M., Zeng, L. M., Zhang, Y. H., Garland, R. M., Su, H., Nowak, A.,
880 Wiedensohler, A., Takegawa, N., Shao, M., and Wahner, A.: Exploring the atmospheric
881 chemistry of nitrous acid (HONO) at a rural site in Southern China, Atmospheric Chemistry
882 and Physics, 12, 1497-1513, 10.5194/acp-12-1497-2012, 2012.
883 Lu, K. D., Rohrer, F., Holland, F., Fuchs, H., Bohn, B., Brauers, T., Chang, C. C., Haseler, R.,
884 Hu, M., Kita, K., Kondo, Y., Li, X., Lou, S. R., Nehr, S., Shao, M., Zeng, L. M., Wahner, A.,
885 Zhang, Y. H., and Hofzumahaus, A.: Observation and modelling of OH and HO2
886 concentrations in the Pearl River Delta 2006: a missing OH source in a VOC rich atmosphere,
887 Atmospheric Chemistry and Physics, 12, 1541-1569, 10.5194/acp-12-1541-2012, 2012.
888 Lu, K. D., Hofzumahaus, A., Holland, F., Bohn, B., Brauers, T., Fuchs, H., Hu, M., Haseler,
889 R., Kita, K., Kondo, Y., Li, X., Lou, S. R., Oebel, A., Shao, M., Zeng, L. M., Wahner, A.,
890 Zhu, T., Zhang, Y. H., and Rohrer, F.: Missing OH source in a suburban environment near
891 Beijing: observed and modelled OH and HO2 concentrations in summer 2006, Atmospheric
892 Chemistry and Physics, 13, 1057-1080, 10.5194/acp-13-1057-2013, 2013.
893 Meng, X.-L., Rosenthal, R., and Rubin, D. B.: Comparing correlated correlation coefficients,
894 Psychological bulletin, 111, 172, 1992.
895 Meng, Z., Lin, W., Jiang, X., Yan, P., Wang, Y., Zhang, Y., Jia, X., and Yu, X.:
896 Characteristics of atmospheric ammonia over Beijing, China, Atmospheric Chemistry and
897 Physics, 11, 6139-6151, 2011.
898 Meusel, H., Kuhn, U., Reiffs, A., Mallik, C., Harder, H., Martinez, M., Schuladen, J., Bohn,
899 B., Parchatka, U., Crowley, J. N., Fischer, H., Tomsche, L., Novelli, A., Hoffmann, T.,
900 Janssen, R. H. H., Hartogensis, O., Pikridas, M., Vrekoussis, M., Bourtsoukidis, E., Weber, B.,
901 Lelieveld, J., Williams, J., Pöschl, U., Cheng, Y., and Su, H.: Daytime formation of nitrous
902 acid at a coastal remote site in Cyprus indicating a common ground source of atmospheric
903 HONO and NO, Atmospheric Chemistry and Physics, 16, 14475-14493,
904 10.5194/acp-16-14475-2016, 2016.
905 Michoud, V., Colomb, A., Borbon, A., Miet, K., Beekmann, M., Camredon, M., Aumont, B.,
906 Perrier, S., Zapf, P., Siour, G., Ait-Helal, W., Afif, C., Kukui, A., Furger, M., Dupont, J. C.,
907 Haeffelin, M., and Doussin, J. F.: Study of the unknown HONO daytime source at a European
908 suburban site during the MEGAPOLI summer and winter field campaigns, Atmospheric
909 Chemistry and Physics, 14, 2805-2822, 10.5194/acp-14-2805-2014, 2014.
910 Nie, W., Ding, A. J., Xie, Y. N., Xu, Z., Mao, H., Kerminen, V. M., Zheng, L. F., Qi, X. M.,
911 Huang, X., Yang, X. Q., Sun, J. N., Herrmann, E., Petäjä, T., Kulmala, M., and Fu, C. B.:
912 Influence of biomass burning plumes on HONO chemistry in eastern China, Atmospheric
913 Chemistry and Physics, 15, 1147-1159, 10.5194/acp-15-1147-2015, 2015.
914 Oswald, R., Behrendt, T., Ermel, M., Wu, D., Su, H., Cheng, Y., Breuninger, C., Moravek, A.,
915 Mougin, E., and Delon, C.: HONO emissions from soil bacteria as a major source of
916 atmospheric reactive nitrogen, Science, 341, 1233-1235, 2013.
917 Pagsberg, P., Bjergbakke, E., Ratajczak, E., and Sillesen, A.: Kinetics of the gas phase

reaction OH+ NO (+ M)→ HONO (+ M) and the determination of the UV absorption cross sections of HONO, Chemical physics letters, 272, 383-390, 1997.

Perner, D., and Platt, U.: Detection of nitrous acid in the atmosphere by differential optical absorption, Geophysical Research Letters, 6, 917-920, doi:10.1029/GL006i012p00917, 1979.

Platt, U., Perner, D., Harris, G. W., Winer, A. M., and Pitts, J. N.: Observations of nitrous acid in an urban atmosphere by differential optical absorption, Nature, 285, 312-314, 10.1038/285312a0, 1980.

Qi, X. M., Ding, A. J., Nie, W., Petäjä, T., Kerminen, V. M., Herrmann, E., Xie, Y. N., Zheng, L. F., Manninen, H., Aalto, P., Sun, J. N., Xu, Z. N., Chi, X. G., Huang, X., Boy, M., Virkkula, A., Yang, X. Q., Fu, C. B., and Kulmala, M.: Aerosol size distribution and new particle formation in the western Yangtze River Delta of China: 2 years of measurements at the SORPES station, Atmospheric Chemistry and Physics, 15, 12445-12464, 10.5194/acp-15-12445-2015, 2015.

Rappenglück, B., Lubertino, G., Alvarez, S., Golovko, J., Czader, B., and Ackermann, L.: Radical precursors and related species from traffic as observed and modeled at an urban highway junction, Journal of the Air & Waste Management Association, 63, 1270-1286, 10.1080/10962247.2013.822438, 2013.

Reisinger, A. R.: Observations of HNO2 in the polluted winter atmosphere: possible heterogeneous production on aerosols, Atmos. Environ., 34, 3865-3874, 2000.

Richter, A., Burrows, J. P., Nuss, H., Granier, C., and Niemeier, U.: Increase in tropospheric nitrogen dioxide over China observed from space, Nature, 437, 129-132, 10.1038/nature04092, 2005.

Rohde, R. A., and Muller, R. A.: Air Pollution in China: Mapping of Concentrations and Sources, PLoS One, 10, e0135749, 10.1371/journal.pone.0135749, 2015.

Rohrer, F., and Berresheim, H.: Strong correlation between levels of tropospheric hydroxyl radicals and solar ultraviolet radiation, Nature, 442, 184-187, 10.1038/nature04924, 2006.

Rohrer, F., Lu, K., Hofzumahaus, A., Bohn, B., Brauers, T., Chang, C.-C., Fuchs, H., Häseler, R., Holland, F., Hu, M., Kita, K., Kondo, Y., Li, X., Lou, S., Oebel, A., Shao, M., Zeng, L., Zhu, T., Zhang, Y., and Wahner, A.: Maximum efficiency in the hydroxyl-radical-based self-cleansing of the troposphere, Nature Geoscience, 7, 559-563, 10.1038/ngeo2199, 2014.

Saliba, N., Yang, H., and Finlayson-Pitts, B.: Reaction of gaseous nitric oxide with nitric acid on silica surfaces in the presence of water at room temperature, The Journal of Physical Chemistry A, 105, 10339-10346, 2001.

Seinfeld, J. H., and Pandis, S. N.: Atmospheric chemistry and physics: from air pollution to climate change, John Wiley & Sons, 2016.

Shao, P., Xin, J., An, J., Kong, L., Wang, B., Wang, J., Wang, Y., and Wu, D.: The empirical relationship between PM2.5 and AOD in Nanjing of the Yangtze River Delta, Atmospheric Pollution Research, 8, 233-243, 10.1016/j.apr.2016.09.001, 2017.

Shen, Y., Virkkula, A., Ding, A., Wang, J., Chi, X., Nie, W., Qi, X., Huang, X., Liu, Q., Zheng, L., Xu, Z., Petäjä, T., Aalto, P. P., Fu, C., and Kulmala, M.: Aerosol optical properties at SORPES in Nanjing, east China, Atmospheric Chemistry and Physics, 18, 5265-5292, 10.5194/acp-18-5265-2018, 2018.

Sleiman, M., Gundel, L. A., Pankow, J. F., Jacob, P., 3rd, Singer, B. C., and Destaillats, H.: Formation of carcinogens indoors by surface-mediated reactions of nicotine with nitrous acid,

962 leading to potential thirdhand smoke hazards, Proc Natl Acad Sci U S A, 107, 6576-6581,
963 10.1073/pnas.0912820107, 2010.

964 Sörgel, M., Regelin, E., Bozem, H., Diesch, J. M., Drewnick, F., Fischer, H., Harder, H., Held,
965 A., Hosaynali-Beygi, Z., Martinez, M., and Zetzsch, C.: Quantification of the unknown
966 HONO daytime source and its relation to NO2, Atmospheric Chemistry and Physics, 11,
967 10433-10447, 10.5194/acp-11-10433-2011, 2011.

968 Stemmler, K., Ammann, M., Donders, C., Kleffmann, J., and George, C.: Photosensitized
969 reduction of nitrogen dioxide on humic acid as a source of nitrous acid, Nature, 440, 195-198,
970 10.1038/nature04603, 2006.

971 Stemmler, K., Ndour, M., Elshorbany, Y., Kleffmann, J., D'anna, B., George, C., Bohn, B.,
972 and Ammann, M.: Light induced conversion of nitrogen dioxide into nitrous acid on
973 submicron humic acid aerosol, Atmospheric Chemistry and Physics, 7, 4237-4248, 2007.

974 Stutz, J., Kim, E. S., Platt, U., Bruno, P., Perrino, C., and Febo, A.: UV-visible absorption
975 cross sections of nitrous acid, Journal of Geophysical Research: Atmospheres, 105,
976 14585-14592, 10.1029/2000jd900003, 2000.

977 Stutz, J., Alicke, B., and Neftel, A.: Nitrous acid formation in the urban atmosphere: Gradient
978 measurements of NO2and HONO over grass in Milan, Italy, Journal of Geophysical Research,
979 107, 10.1029/2001jd000390, 2002.

980 Stutz, J., Alicke, B., Ackermann, R., Geyer, A., Wang, S., White, A. B., Williams, E. J.,
981 Spicer, C. W., and Fast, J. D.: Relative humidity dependence of HONO chemistry in urban
982 areas, Journal of Geophysical Research: Atmospheres, 109, n/a-n/a, 10.1029/2003jd004135,
983 2004.

984 Su, H., Cheng, Y. F., Cheng, P., Zhang, Y. H., Dong, S., Zeng, L. M., Wang, X., Slanina, J.,
985 Shao, M., and Wiedensohler, A.: Observation of nighttime nitrous acid (HONO) formation at
986 a non-urban site during PRIDE-PRD2004 in China, Atmos. Environ., 42, 6219-6232,
987 10.1016/j.atmosenv.2008.04.006, 2008a.

988 Su, H., Cheng, Y. F., Shao, M., Gao, D. F., Yu, Z. Y., Zeng, L. M., Slanina, J., Zhang, Y. H.,
989 and Wiedensohler, A.: Nitrous acid (HONO) and its daytime sources at a rural site during the
990 2004 PRIDE-PRD experiment in China, Journal of Geophysical Research, 113,
991 10.1029/2007jd009060, 2008b.

992 Su, H., Cheng, Y., Oswald, R., Behrendt, T., Trebs, I., Meixner, F. X., Andreae, M. O., Cheng,
993 P., Zhang, Y., and Pöschl, U.: Soil nitrite as a source of atmospheric HONO and OH radicals,
994 Science, 333, 1616-1618, 2011.

995 Sumner, A. L., Menke, E. J., Dubowski, Y., Newberg, J. T., Penner, R. M., Hemminger, J. C.,
996 Wingen, L. M., Brauers, T., and Finlayson-Pitts, B. J.: The nature of water on surfaces of
997 laboratory systems and implications for heterogeneous chemistry in the troposphere, Physical
998 Chemistry Chemical Physics, 6, 10.1039/b308125g, 2004.

999 Sun, P., Nie, W., Chi, X., Xie, Y., Huang, X., Xu, Z., Qi, X., Xu, Z., Wang, L., Wang, T.,
1000 Zhang, Q., and Ding, A.: Two years of online measurement of fine particulate nitrate in the
1001 western Yangtze River Delta: influences of thermodynamics and
1002 N$_2$O$_5$ hydrolysis, Atmospheric Chemistry
1003 and Physics, 18, 17177-17190, 10.5194/acp-18-17177-2018, 2018.

1004 Tan, Z., Fuchs, H., Lu, K., Hofzumahaus, A., Bohn, B., Broch, S., Dong, H., Gomm, S.,
1005 Haeseler, R., He, L., Holland, F., Li, X., Liu, Y., Lu, S., Rohrer, F., Shao, M., Wang, B.,

Wang, M., Wu, Y., Zeng, L., Zhang, Y., Wahner, A., and Zhang, Y.: Radical chemistry at a rural site (Wangdu) in the North China Plain: observation and model calculations of OH, HO2 and RO2 radicals, Atmospheric Chemistry and Physics, 17, 663-690, 10.5194/acp-17-663-2017, 2017.

Tan, Z., Rohrer, F., Lu, K., Ma, X., Bohn, B., Broch, S., Dong, H., Fuchs, H., Gkatzelis, G. I., Hofzumahaus, A., Holland, F., Li, X., Liu, Y., Liu, Y., Novelli, A., Shao, M., Wang, H., Wu, Y., Zeng, L., Hu, M., Kiendler-Scharr, A., Wahner, A., and Zhang, Y.: Wintertime photochemistry in Beijing: observations of ROx radical concentrations in the North China Plain during the BEST-ONE campaign, Atmospheric Chemistry and Physics, 18, 12391-12411, 10.5194/acp-18-12391-2018, 2018.

Tong, S., Hou, S., Zhang, Y., Chu, B., Liu, Y., He, H., Zhao, P., and Ge, M.: Comparisons of measured nitrous acid (HONO) concentrations in a pollution period at urban and suburban Beijing, in autumn of 2014, Science China Chemistry, 58, 1393-1402, 10.1007/s11426-015-5454-2, 2015.

Underwood, G., Song, C., Phadnis, M., Carmichael, G., and Grassian, V.: Heterogeneous reactions of NO2 and HNO3 on oxides and mineral dust: A combined laboratory and modeling study, Journal of Geophysical Research: Atmospheres, 106, 18055-18066, 2001.

VandenBoer, T., Markovic, M., Sanders, J., Ren, X., Pusede, S., Browne, E., Cohen, R., Zhang, L., Thomas, J., and Brune, W.: Evidence for a nitrous acid (HONO) reservoir at the ground surface in Bakersfield, CA, during CalNex 2010, Journal of Geophysical Research: Atmospheres, 119, 9093-9106, 2014a.

VandenBoer, T. C., Young, C. J., Talukdar, R. K., Markovic, M. Z., Brown, S. S., Roberts, J. M., and Murphy, J. G.: Nocturnal loss and daytime source of nitrous acid through reactive uptake and displacement, Nature Geoscience, 8, 55-60, 10.1038/ngeo2298, 2014b.

Villena, G., Kleffmann, J., Kurtenbach, R., Wiesen, P., Lissi, E., Rubio, M. A., Croxatto, G., and Rappenglück, B.: Vertical gradients of HONO, NOx and O3 in Santiago de Chile, Atmos. Environ., 45, 3867-3873, 10.1016/j.atmosenv.2011.01.073, 2011a.

Villena, G., Wiesen, P., Cantrell, C. A., Flocke, F., Fried, A., Hall, S. R., Hornbrook, R. S., Knapp, D., Kosciuch, E., Mauldin, R. L., McGrath, J. A., Montzka, D., Richter, D., Ullmann, K., Walega, J., Weibring, P., Weinheimer, A., Staebler, R. M., Liao, J., Huey, L. G., and Kleffmann, J.: Nitrous acid (HONO) during polar spring in Barrow, Alaska: A net source of OH radicals?, Journal of Geophysical Research, 116, 10.1029/2011jd016643, 2011b.

Wang, G., Zhang, R., Gomez, M. E., Yang, L., Levy Zamora, M., Hu, M., Lin, Y., Peng, J., Guo, S., Meng, J., Li, J., Cheng, C., Hu, T., Ren, Y., Wang, Y., Gao, J., Cao, J., An, Z., Zhou, W., Li, G., Wang, J., Tian, P., Marrero-Ortiz, W., Secrest, J., Du, Z., Zheng, J., Shang, D., Zeng, L., Shao, M., Wang, W., Huang, Y., Wang, Y., Zhu, Y., Li, Y., Hu, J., Pan, B., Cai, L., Cheng, Y., Ji, Y., Zhang, F., Rosenfeld, D., Liss, P. S., Duce, R. A., Kolb, C. E., and Molina, M. J.: Persistent sulfate formation from London Fog to Chinese haze, Proc Natl Acad Sci U S A, 113, 13630-13635, 10.1073/pnas.1616540113, 2016.

Wang, J., Zhang, X., Guo, J., Wang, Z., and Zhang, M.: Observation of nitrous acid (HONO) in Beijing, China: Seasonal variation, nocturnal formation and daytime budget, Sci Total Environ, 587-588, 350-359, 10.1016/j.scitotenv.2017.02.159, 2017.

Wang, S.: Atmospheric observations of enhanced NO2-HONO conversion on mineral dust particles, Geophysical Research Letters, 30, 10.1029/2003gl017014, 2003.

1050   Wang, S., Zhou, R., Zhao, H., Wang, Z., Chen, L., and Zhou, B.: Long-term observation of
1051   atmospheric nitrous acid (HONO) and its implication to local NO2 levels in Shanghai, China,
1052   Atmos. Environ., 77, 718-724, 10.1016/j.atmosenv.2013.05.071, 2013.

1053   Wentzell, J. J. B., Schiller, C. L., and Harris, G. W.: Measurements of HONO during
1054   BAQS-Met, Atmospheric Chemistry and Physics, 10, 12285-12293,
1055   10.5194/acp-10-12285-2010, 2010.

1056   Wong, K. W., Oh, H. J., Lefer, B. L., Rappenglück, B., and Stutz, J.: Vertical profiles of
1057   nitrous acid in the nocturnal urban atmosphere of Houston, TX, Atmospheric Chemistry and
1058   Physics, 11, 3595-3609, 10.5194/acp-11-3595-2011, 2011.

1059   Xie, Y., Ding, A., Nie, W., Mao, H., Qi, X., Huang, X., Xu, Z., Kerminen, V.-M., Petäjä, T.,
1060   Chi, X., Virkkula, A., Boy, M., Xue, L., Guo, J., Sun, J., Yang, X., Kulmala, M., and Fu, C.:
1061   Enhanced sulfate formation by nitrogen dioxide: Implications from in situ observations at the
1062   SORPES station, Journal of Geophysical Research: Atmospheres, 120, 12679-12694,
1063   10.1002/2015jd023607, 2015.

1064   Xu, Z., Wang, T., Xue, L. K., Louie, P. K. K., Luk, C. W. Y., Gao, J., Wang, S. L., Chai, F.
1065   H., and Wang, W. X.: Evaluating the uncertainties of thermal catalytic conversion in
1066   measuring atmospheric nitrogen dioxide at four differently polluted sites in China, Atmos.
1067   Environ., 76, 221-226, 10.1016/j.atmosenv.2012.09.043, 2013.

1068   Xu, Z., Wang, T., Wu, J., Xue, L., Chan, J., Zha, Q., Zhou, S., Louie, P. K. K., and Luk, C. W.
1069   Y.: Nitrous acid (HONO) in a polluted subtropical atmosphere: Seasonal variability, direct
1070   vehicle emissions and heterogeneous production at ground surface, Atmos. Environ., 106,
1071   100-109, 10.1016/j.atmosenv.2015.01.061, 2015.

1072   Xu, Z., Huang, X., Nie, W., Chi, X., Xu, Z., Zheng, L., Sun, P., and Ding, A.: Influence of
1073   synoptic condition and holiday effects on VOCs and ozone production in the Yangtze River
1074   Delta region, China, Atmos. Environ., 168, 112-124, 10.1016/j.atmosenv.2017.08.035, 2017.

1075   Xu, Z., Huang, X., Nie, W., Shen, Y., Zheng, L., Xie, Y., Wang, T., Ding, K., Liu, L., Zhou,
1076   D., Qi, X., and Ding, A.: Impact of Biomass Burning and Vertical Mixing of Residual-Layer
1077   Aged Plumes on Ozone in the Yangtze River Delta, China: A Tethered-Balloon Measurement
1078   and Modeling Study of a Multiday Ozone Episode, Journal of Geophysical Research:
1079   Atmospheres, 123, 11,786-711,803, 10.1029/2018jd028994, 2018.

1080   Yabushita, A., Enami, S., Sakamoto, Y., Kawasaki, M., Hoffmann, M. R., and Colussi, A. J.:
1081   Anion-Catalyzed Dissolution of NO2 on Aqueous Microdroplets, J. Phys. Chem. A, 113,
1082   4844-4848, 10.1021/jp900685f, 2009.

1083   Ye, C., Zhou, X., Pu, D., Stutz, J., Festa, J., Spolaor, M., Tsai, C., Cantrell, C., Mauldin, R. L.,
1084   3rd, Campos, T., Weinheimer, A., Hornbrook, R. S., Apel, E. C., Guenther, A., Kaser, L.,
1085   Yuan, B., Karl, T., Haggerty, J., Hall, S., Ullmann, K., Smith, J. N., Ortega, J., and Knote, C.:
1086   Rapid cycling of reactive nitrogen in the marine boundary layer, Nature, 532, 489-491,
1087   10.1038/nature17195, 2016.

1088   Ye, C., Zhang, N., Gao, H., and Zhou, X.: Photolysis of Particulate Nitrate as a Source of
1089   HONO and NOx, Environ Sci Technol, 51, 6849-6856, 10.1021/acs.est.7b00387, 2017.

1090   Yu, Y., Galle, B., Panday, A., Hodson, E., Prinn, R., and Wang, S.: Observations of high rates
1091   of NO2-HONO conversion in the nocturnal atmospheric boundary layer in Kathmandu, Nepal,
1092   ATMOSPHERIC CHEMISTRY AND PHYSICS, 9, 6401-6415, 10.5194/acp-9-6401-2009,
1093   2009.

Zhou, L., Wang, W., Hou, S., Tong, S., and Ge, M.: Heterogeneous uptake of nitrogen dioxide on Chinese mineral dust, J Environ Sci (China), 38, 110-118, 10.1016/j.jes.2015.05.017, 2015.

Zhou, X., Civerolo, K., Dai, H., Huang, G., Schwab, J., and Demerjian, K.: Summertime nitrous acid chemistry in the atmospheric boundary layer at a rural site in New York State, Journal of Geophysical Research: Atmospheres, 107, ACH 13-11-ACH 13-11, 10.1029/2001jd001539, 2002.

Zhou, X., Gao, H., He, Y., Huang, G., Bertman, S. B., Civerolo, K., and Schwab, J.: Nitric acid photolysis on surfaces in low-NOxenvironments: Significant atmospheric implications, Geophysical Research Letters, 30, n/a-n/a, 10.1029/2003gl018620, 2003.

Zhou, X., Zhang, N., TerAvest, M., Tang, D., Hou, J., Bertman, S., Alaghmand, M., Shepson, P. B., Carroll, M. A., Griffith, S., Dusanter, S., and Stevens, P. S.: Nitric acid photolysis on forest canopy surface as a source for tropospheric nitrous acid, Nature Geoscience, 4, 440-443, 10.1038/ngeo1164, 2011.

Tables

Table 1. Sources and sinks for nitrous acid (HONO) in the troposphere.

Budget	Occurrence	Pathways	Abbr.
Sinks	Only daytime	$HONO + h\upsilon \xrightarrow{320-400nm} OH + NO$	R1
	Mainly daytime	$HONO + OH \rightarrow NO_2 + H_2O$	R2
	All day	Deposition/heterogeneous loss on aerosol	/
Sources	Mainly daytime	$NO + OH \xrightarrow{M} HONO$	R3
	Mainly nighttime	$2NO_{2(g)} + H_2O_{(ads)} \xrightarrow{surf} HONO_{(g)} + HNO_{3(ads)}$	R4
	Mainly daytime	$NO_{2(g)} + HC_{red} \xrightarrow{surf} HONO_{(g)} + HC_{ox}$	R5
	Only daytime	$HNO_3 / NO_3^- + h\upsilon \xrightarrow{surf} HONO / NO_2^- + O$	R6
	All day	Release of soil nitrite	/
	All day	Combustion emission(fossil and biomass)	/

Table 2. Overview of the measured HONO and NOx levels in Nanjing and comparison with other urban or suburban sites.

Location	Date	HONO(ppb)		NO$_2$(ppb)		NOx(ppb)		HONO/NO2		HONO/NOx		Ref
		Night	Day	Night	Day	Night	Day	Night	Day	Night	Day	
Rome(Italy)	May-Jun 2001	1.00	0.15	27.2	4.0	51.2	4.2	0.037	0.038	0.020	0.036	1
Kathmandu(Nepal)	Jan-Feb 2003	1.74	0.35	17.9	8.6	20.1	13.0	0.097	0.041	0.087	0.027	2
Tokto(Japan)	Jan-Feb 2004	0.80	0.05	31.8	18.2	37.4	26.3	0.025	0.003	0.021	0.002	3
Santiago(Chile)	Mar 2005	3.00	1.50	30.0	20.0	200.0	40.0	0.100	0.075	0.015	0.038	4
Mexico City(Mexico)	Mar 2006	/	0.43	/	28.4	/	44.8	/	0.015	/.	0.010	5
Houston(USA)	Sep 2006	0.50	0.10	20.0	10.0	/	/	0.025	0.010	/	/	6
Shanghai(China)	Oct 2009	1.50	1.00	41.9	30.0	/	/	0.038	0.032	/	/	7
Hongkong(China)	Aug 2011	0.66	0.70	21.8	18.1	29.3	29.3	0.031	0.042	0.025	0.028	8
	Nov 2011	0.95	0.89	27.2	29.0	37.2	40.6	0.034	0.030	0.028	0.021	
	Feb 2012	0.88	0.92	22.2	25.8	37.8	48.3	0.036	0.035	0.025	0.020	
	May 2012	0.33	0.40	14.7	15.0	19.1	21.1	0.022	0.030	0.019	0.022	
Beijing(China)	Oct–Nov 2014	1.75	0.93	37.6	35.3	94.5	53.4	0.047	0.026	0.019	0.017	9
Xi'an(China)	Jul–Aug 2015	0.51	1.57	15.4	24.7	/	/	0.033	0.062	/	/	10
Jinan(China)	Sep–Nov 2015	0.87	0.66	25.4	23.2	38.0	37.5	0.049	0.034	0.034	0.022	11
	Dec 2015-Feb 2016	2.15	1.35	41.1	34.6	78.5	64.8	0.056	0.047	0.034	0.031	
	Mar–May 2016	1.24	1.04	35.8	25.8	47.3	36.0	0.046	0.052	0.035	0.041	
	Jun–Aug 2016	1.20	1.01	22.5	19.0	29.1	25.8	0.106	0.079	0.060	0.049	
Nanjing(China)	Nov 2017-Nov 2018	0.80	0.57	18.9	13.9	24.9	19.3	0.045	0.044	0.041	0.036	this
	Dec-Feb(winter)	1.15	0.92	28.4	23.1	45.5	37.7	0.040	0.038	0.029	0.025	study
	Mar–May(spring)	0.76	0.59	17.4	12.9	19.1	15.9	0.048	0.049	0.046	0.042	
	Jun–Aug(summer)	0.56	0.34	12.5	7.7	13.5	9.1	0.048	0.051	0.046	0.045	
	Sep–Nov(autumn)	0.81	0.51	18.9	13.4	25.1	17.7	0.044	0.035	0.039	0.029	

1: Acker et al. (2006); 2: Yu et al. (2009); 3: Kanaya et al. (2007); 4: Elshorbany et al. (2009); 5: Dusanter et al. (2009); 6: Wong et al. (2011); 7: Bernard et al. (2016); 8: Xu et al. (2015); 9: Tong et al. (2015); 10: Huang et al. (2017); 11: Li et al. (2018)

Table 3. Correlations of $P_{unknown}$ against various parameters.

Parameters	Winter		Spring		Summer		Autumn	
	r	N	r	N	r	N	r	N
NO_2	0.46	220	0.33	280	0.07	366	0.15	348
$PM_{2.5}$	0.41	220	0.43	280	0.22	366	0.26	348
NO_3^-	0.39	211	0.41	270	-0.01	353	0.19	344
SO_4^{2-}	0.34	204	0.26	270	0.15	357	0.23	337
NH_4^+	0.38	211	0.36	273	0.09	360	0.22	332
RH	0.00	220	-0.33	280	-0.37	366	-0.19	348
UVB	0.22	220	0.44	280	0.43	366	0.45	348
$NO_2*PM_{2.5}$	0.42	220	0.43	280	0.10	366	0.23	348
$NO_2*NO_3^-$	0.40	211	0.43	270	-0.04	353	0.20	344
$NO_2*SO_4^{2-}$	0.41	204	0.35	270	0.08	357	0.22	337
$NO_2*NH_4^+$	0.41	211	0.41	273	0.05	360	0.21	332
$UVB*NO_2$	0.59	220	0.68	280	0.49	366	0.65	348
$UVB*PM_{2.5}$	0.53	220	0.64	280	0.51	366	0.65	348
$UVB*NO_3^-$	0.50	211	0.56	270	0.25	353	0.46	344
$UVB*SO_4^{2-}$	0.42	204	0.49	270	0.42	357	0.55	337
$UVB*NH_4^+$	0.47	211	0.53	273	0.35	360	0.52	332
$NO_2*UVB*PM_{2.5}$	0.53	220	0.64	280	0.39	366	0.55	348

Figures
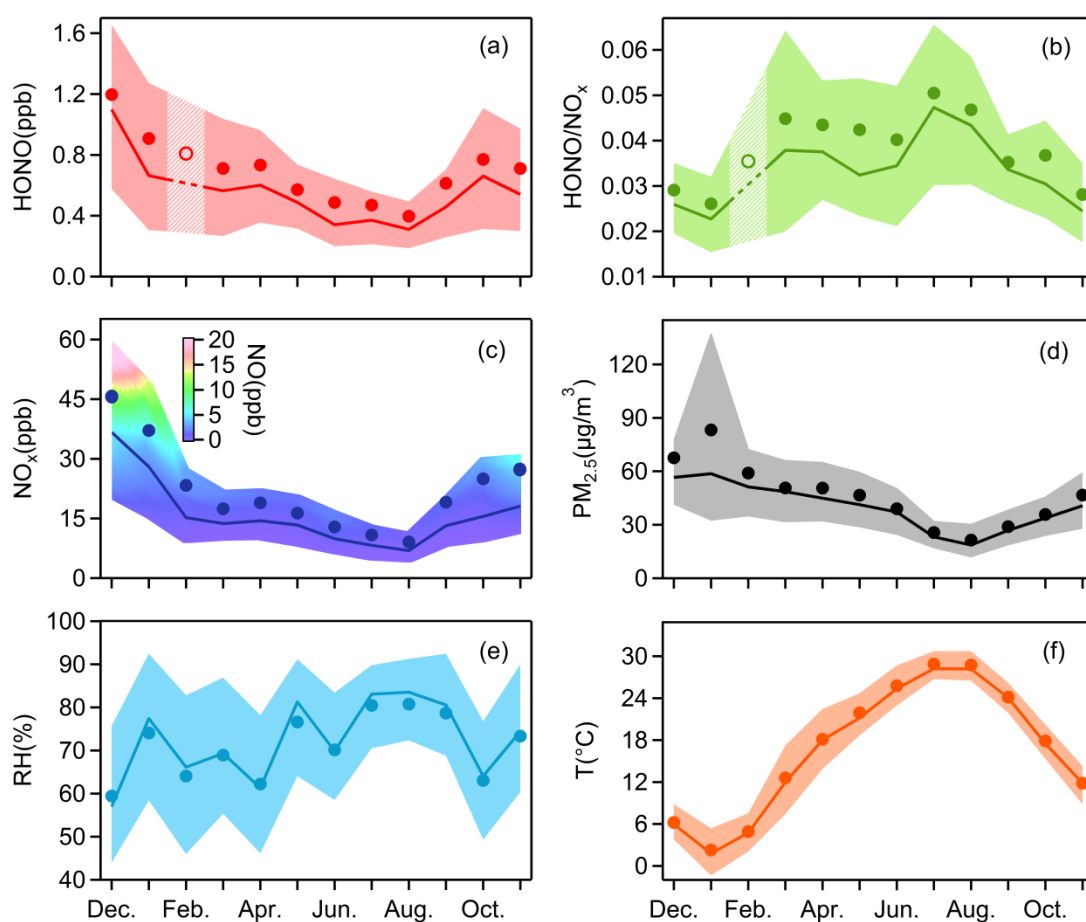
Fig. 1. Monthly variations of (a) HONO, (b) HONO/NO$_x$, (c) NO$_x$, (d) PM$_{2.5}$, (e) RH and (f) T. The solid bold lines are median values, the markers indicate mean values, and the shaded areas represent percentiles of 75% and 25%. In (a) and (b), values in February are linearly interpolated based on the data from the months before and after, since there were only few days when HONO was observed in February. In (c), the shaded area is colored by the 25$_{th}$ to the 75$_{th}$ percentiles of NO.
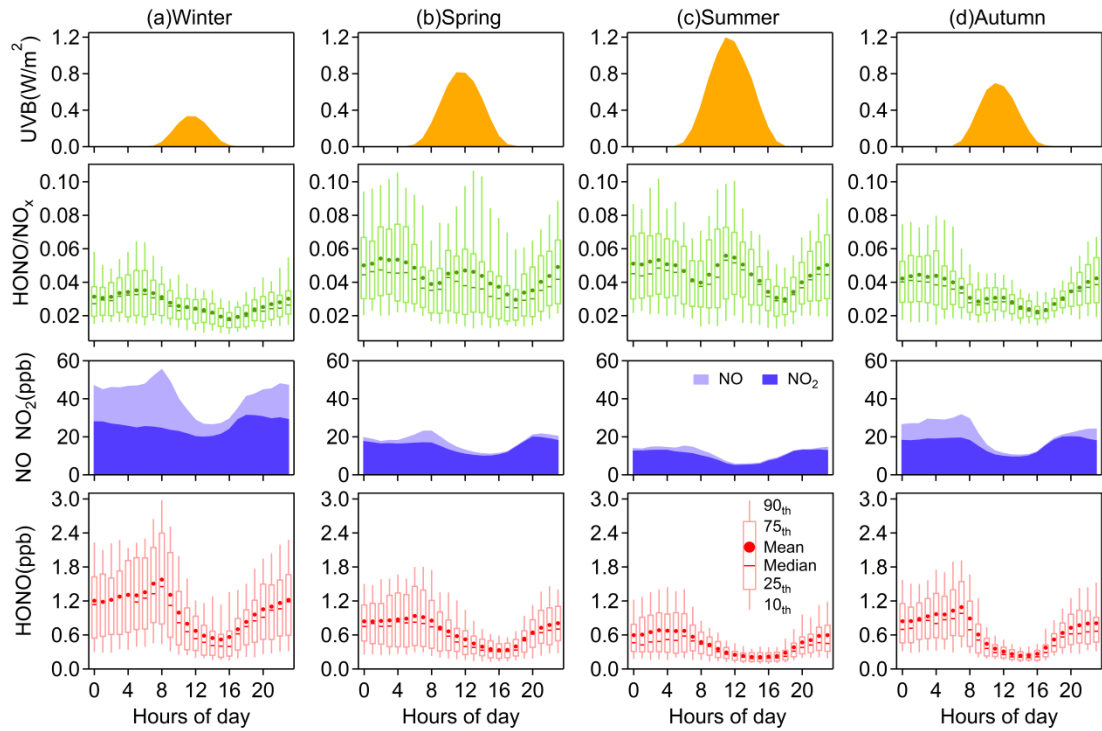
1159
1160 **Fig. 2.** Diurnal variations of HONO, NO, NO_2, HONO/NO_x, UVB in (a) winter, (b) spring, (c)
1161 summer, (d) autumn. The levels of NO, NO_2 and UVB are displayed as their mean concentrations.
1162
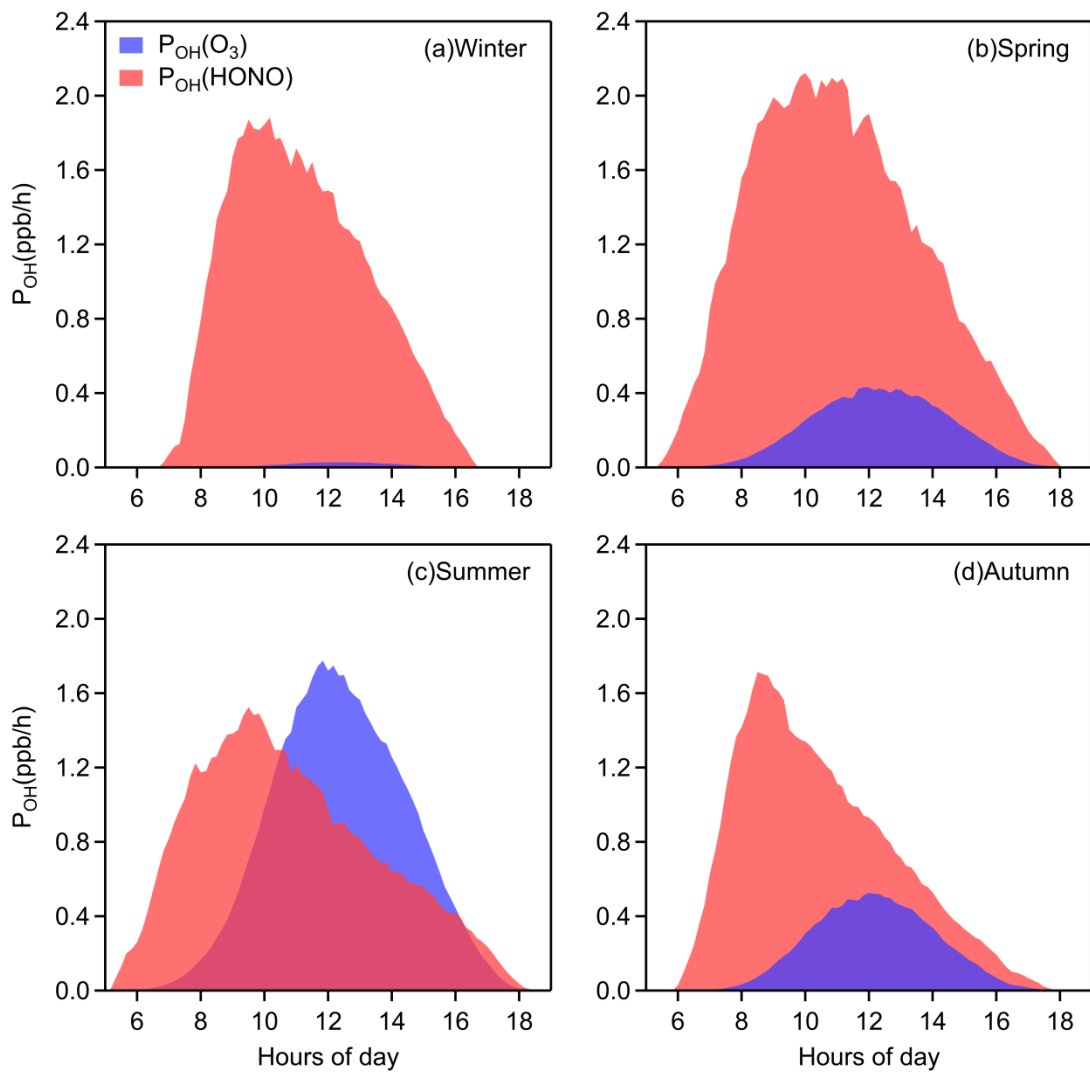
1163
1164 **Fig. 3.** Averaged OH production rates from photolysis of HONO and ozone in (a) winter, (b)
1165 spring, (c) summer, and (d) autumn.

1166
1167
1168
1169
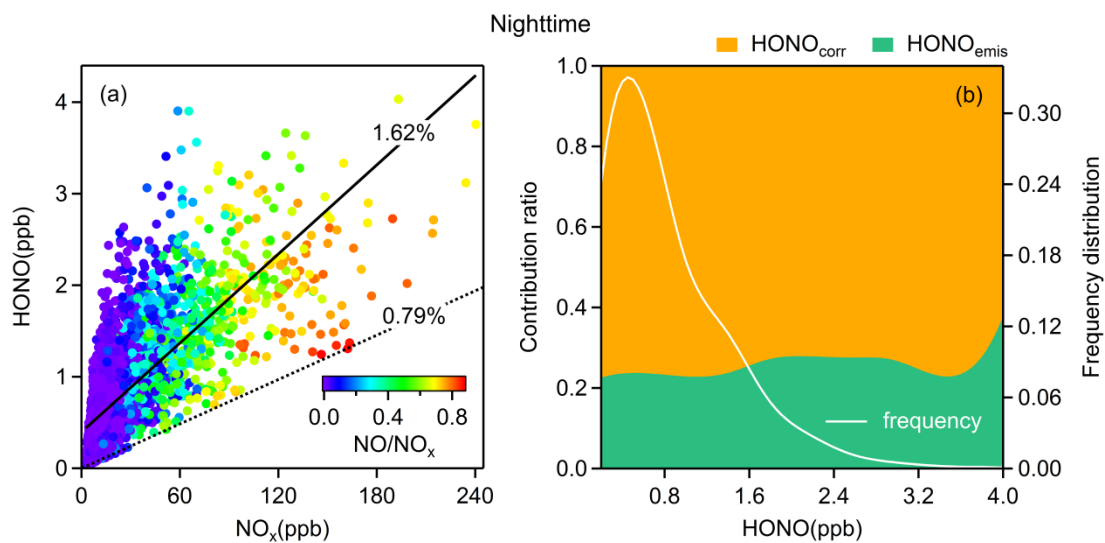
Fig. 4. (a) The relationship between HONO and NO_x colored by the NO/NO_x ratio. The dotted line is the emission ratio derived in this study and the solid line is obtained from simple linear fitting; (b) average emission contribution ratios for different concentrations of HONO and the frequency distribution of HONO concentrations. Both (a) and (b) are nighttime values.
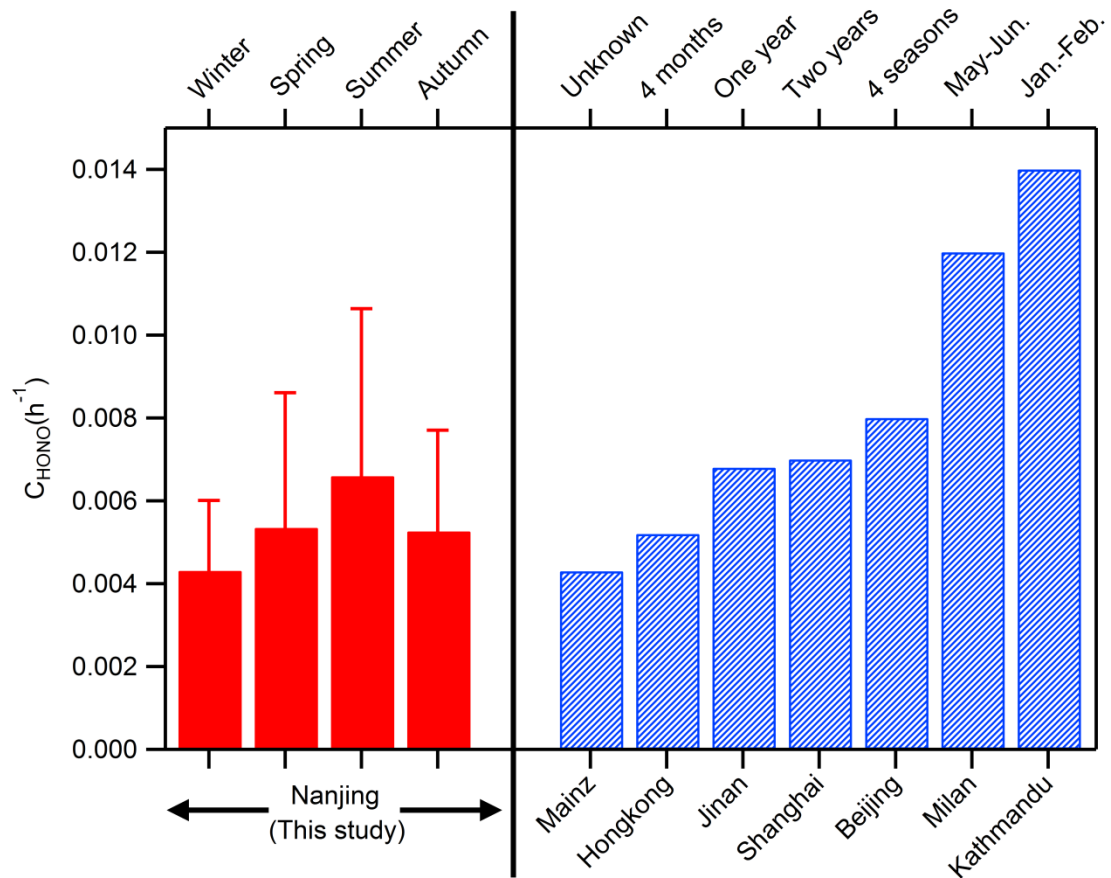
1183

Fig. 5. Comparison of observed NO_2 to HONO conversion rates in cities: Nanjing (this study); Mainz (Lammel, 1999); Hongkong (Xu et al., 2015); Jinan (Li et al., 2018); Shanghai (Wang et al., 2013); Beijing (Wang et al., 2017); Milan (Alicke et al., 2002); and Kathmandu (Yu et al., 2009).
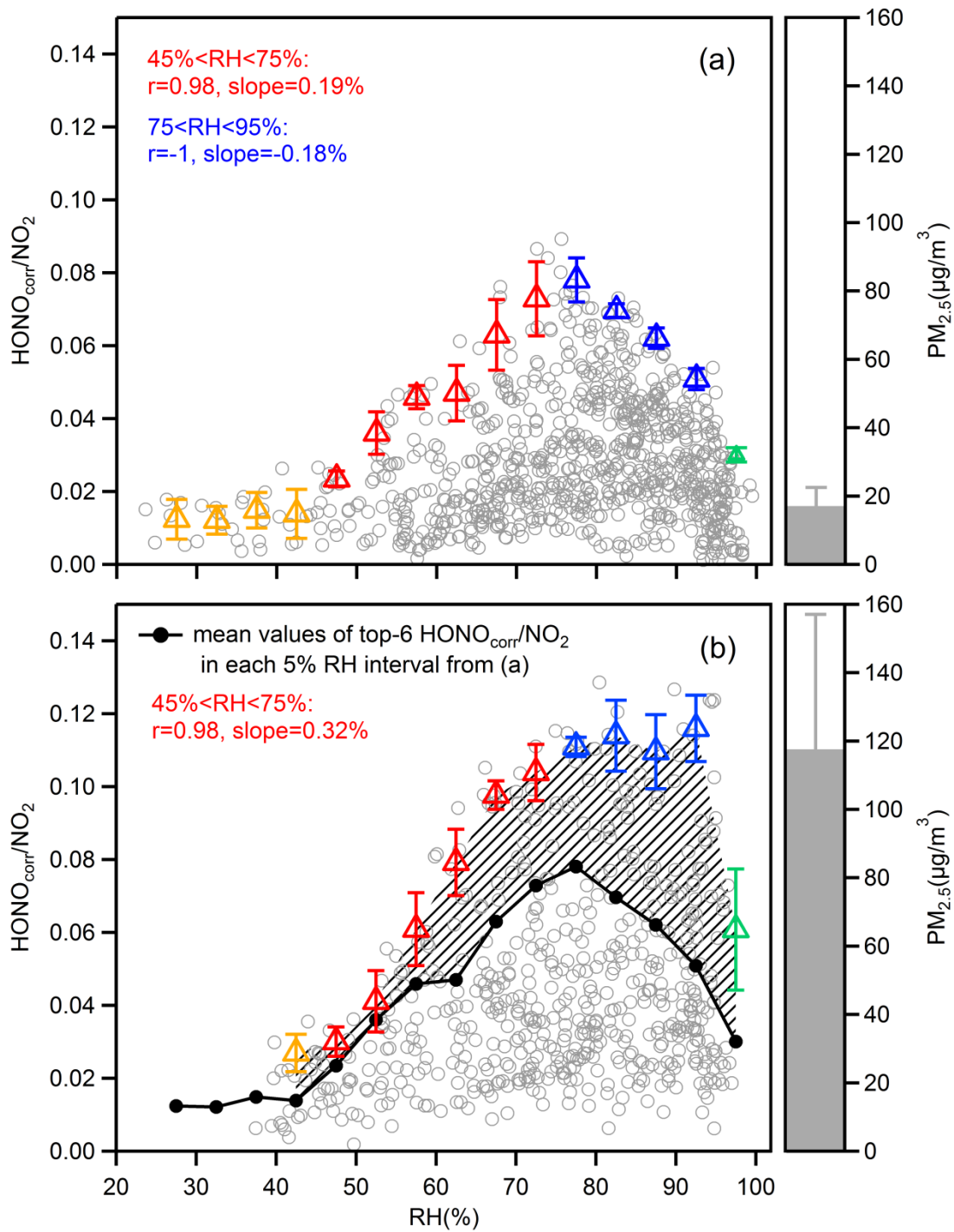
Fig. 6. Scatter plot of the $HONO_{corr}/NO_2$ ratio and RH during nighttime, separating the data into (a) clean hours (hourly mean $PM_{2.5}<25\mu g/m^3$) and (b) polluted hours (hourly mean $PM_{2.5}>75\mu g/m^3$). Triangles are the averaged top-6 $HONO_{corr}/NO2$ in each 5% RH interval, and the error bars are the standard deviations. The overall average concentrations of $PM_{2.5}$ in (a) and (b) are shown to the right of the figures.
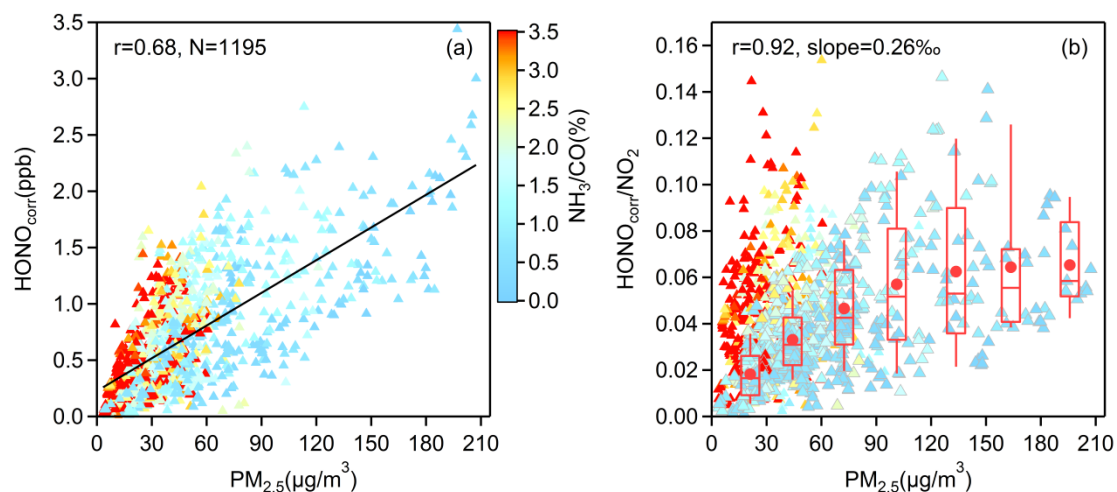
Fig. 7. (a) The correlation between HONO$_{corr}$ and PM$_{2.5}$, and (b) the correlation between HONO$_{corr}$/NO$_2$ and PM$_{2.5}$, all scatters come from the time (3:00-6:00 LT) when the HONO$_{corr}$/NO$_2$ ratio reaches the pseudo steady state at each night and are colored by NH$_3$/CO. In (b), the larger triangles with gray borders, depict the measured data from November to May, and the boxplot in each 30 μg/m^3 interval of PM$_{2.5}$ is illustrated according to the same data, the red box boundaries represent interquartile range, the whiskers represent the 10%–90% percentile range, the horizontal red lines represent median values and the red markers represent mean values. The correlation coefficient and the slope of the linearly fitted line in (b) are derived from the averaged HONO$_{corr}$/NO$_2$ and averaged PM$_{2.5}$ in each box.

1184
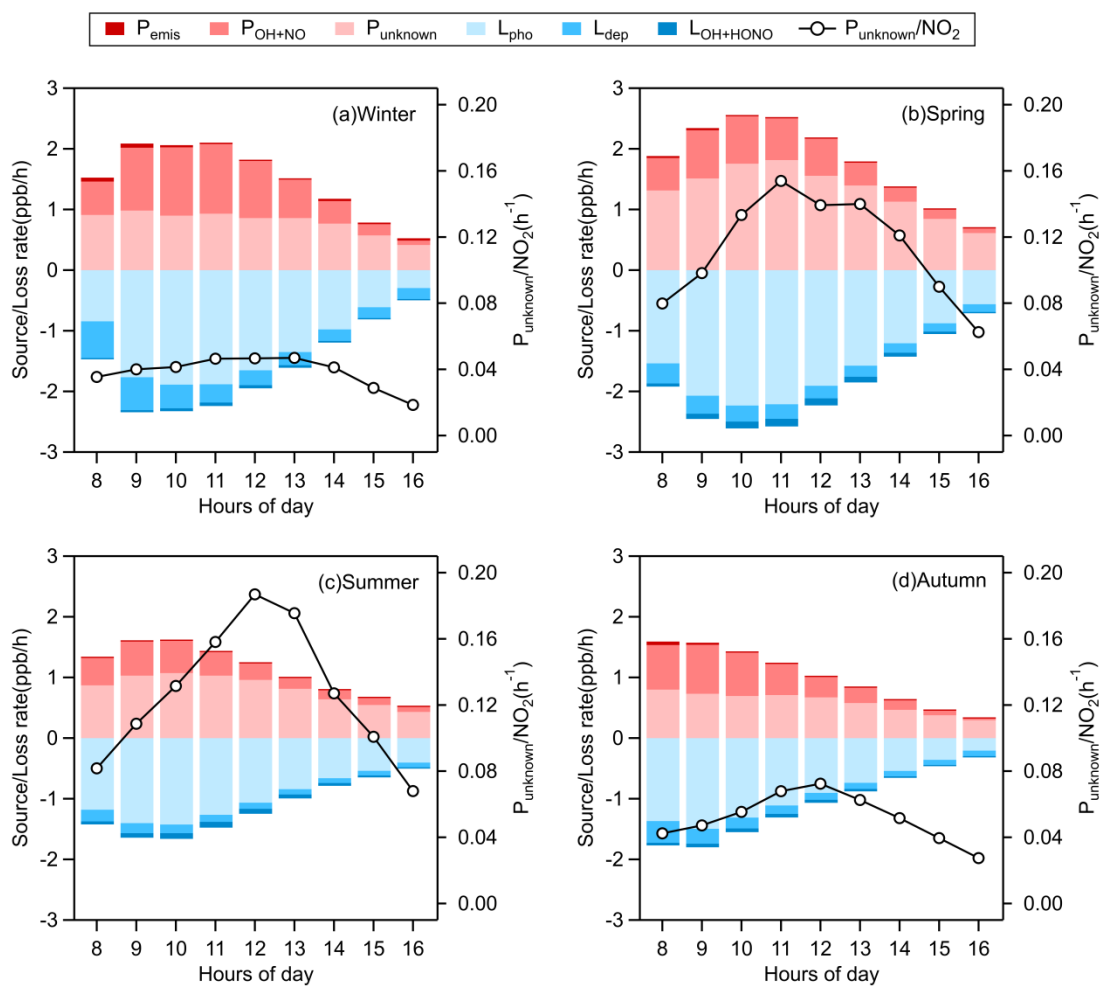
Fig. 8. Averaged daytime HONO budget and the missing source strength ($P_{unknown}$) normalized by NO_2 in (a) winter, (b) spring, (c) summer, and (d) autumn. The mean values of $P_{unknown}$ around noontime (10:00-14:00 LT) are: 0.91 ppb/h in winter, 1.61 ppb/h in Spring, 0.98 ppb/h in summer, 0.68 ppb/h in autumn.
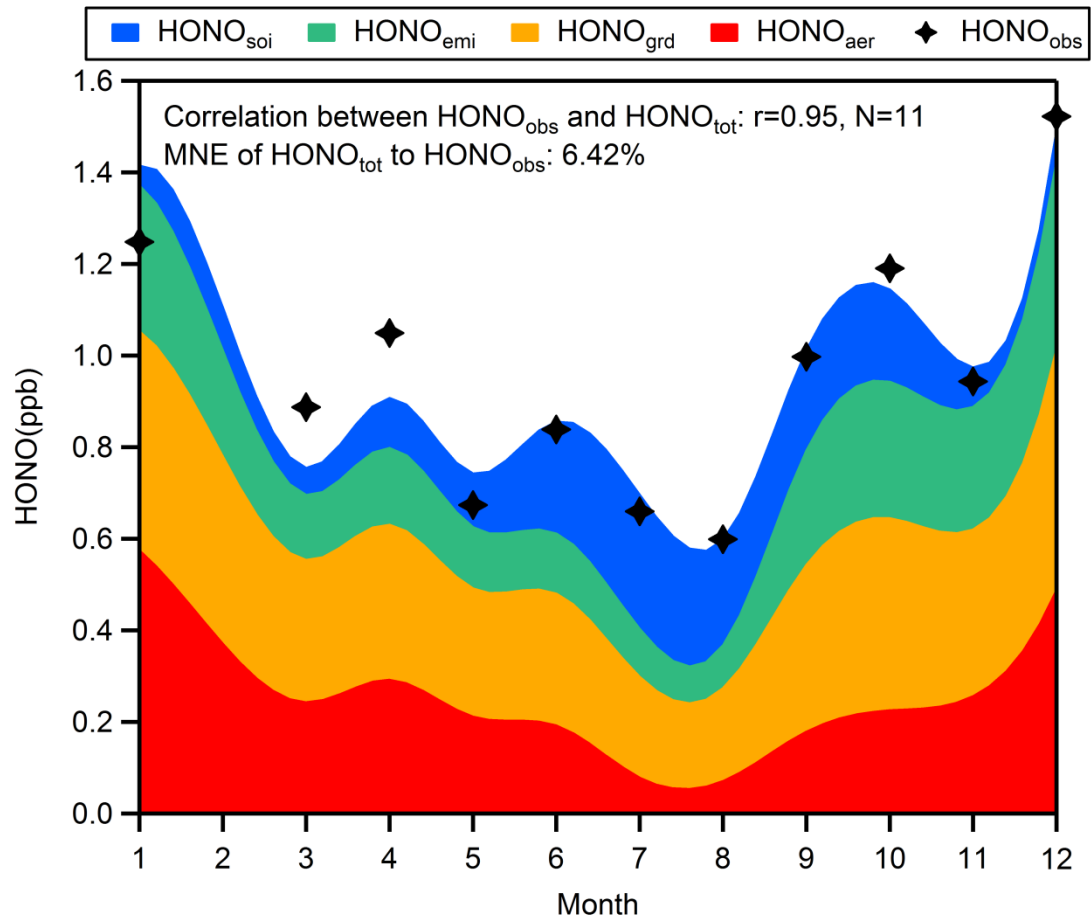
Fig. 9. Seasonal variations of 4 sources of HONO at night (3:00-6:00 LT).The mean normalized error (MNE) of HONO$_{tot}$ to HONO$_{obs}$ is 6.42%.